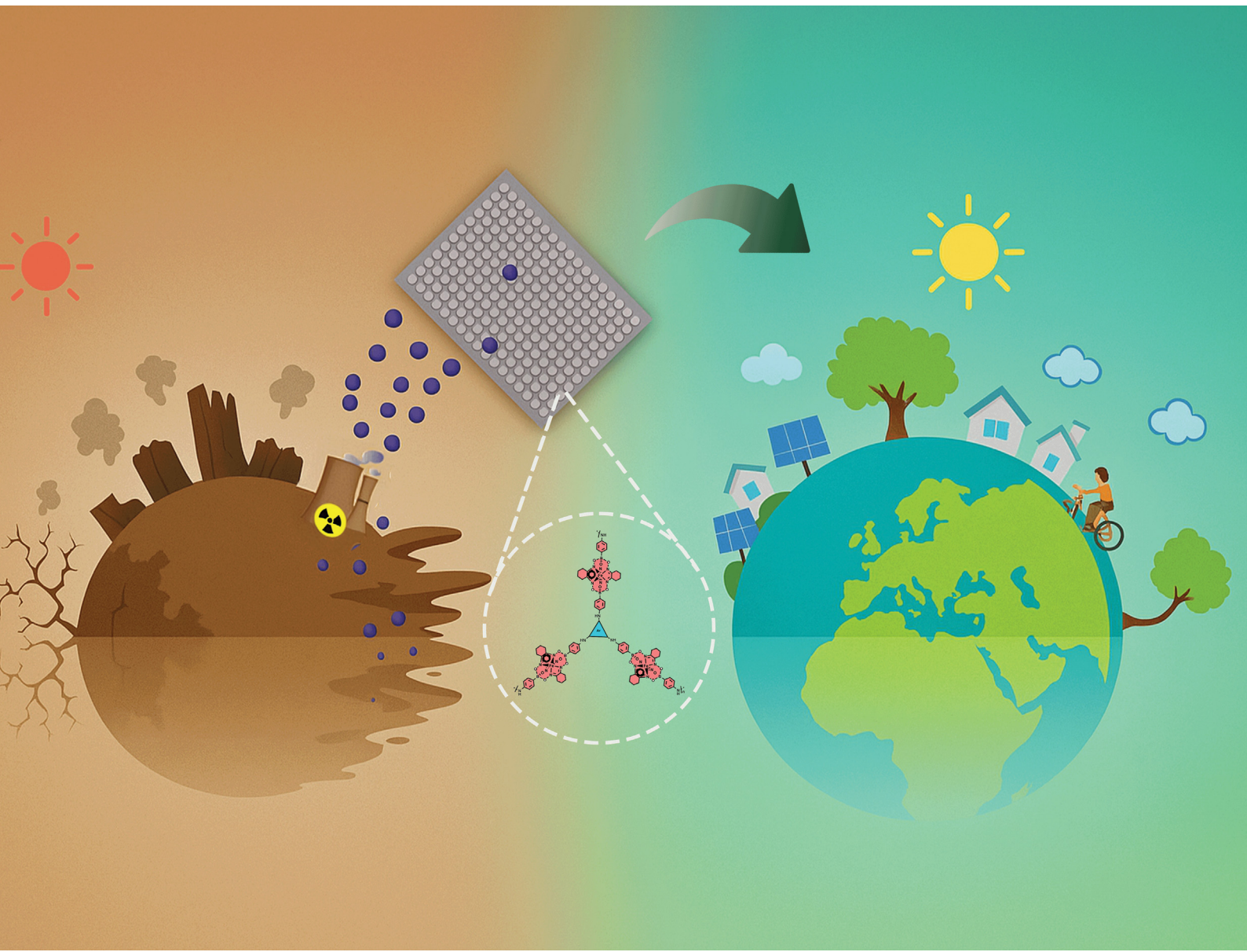


Materials Advances

rsc.li/materials-advances



ISSN 2633-5409

PAPER

Bassam Alameddine *et al.*

High-capacity iodine adsorption from diverse media using iron-based metal-organic copolymer networks synthesized via a microwave-assisted Buchwald-Hartwig cross-coupling reaction



Cite this: *Mater. Adv.*, 2025, 6, 3479

High-capacity iodine adsorption from diverse media using iron-based metal–organic copolymer networks synthesized via a microwave-assisted Buchwald–Hartwig cross-coupling reaction†

Suchetha Shetty, ^{ab} Noorullah Baig, ^{ab} Badvel Pallavi, ^{ab} Rupa Bargakshatriya, ^c Sumit Kumar Pramanik ^c and Bassam Alameddine ^{ab}

Three-dimensional iron(II) clathrochelate-bridged secondary arylamine copolymers (**TAC1–3**) were synthesized via a facile microwave-assisted Buchwald–Hartwig cross-coupling reaction, utilizing a custom-designed diamine clathrochelate precursor along with a range of tribrominated aryl surrogates. The target copolymers exhibited impressive iodine vapor adsorption capabilities, with **TAC3** achieving an outstanding uptake of 1500 wt% (15 g g⁻¹). Kinetic analysis identified a predominant pseudo-2nd-order adsorption model, whilst recyclability tests confirmed the materials' durability, sustaining high efficiency albeit over multiple adsorption–desorption cycles. The **TAC1–3** copolymers demonstrated notable iodine uptake from cyclohexane solutions with **TAC3** achieving a maximum capacity of 1.11 g g⁻¹ at an initial iodine concentration of 1000 mg L⁻¹. Moreover, **TAC1–3** demonstrated exceptional performance in aqueous systems, achieving adsorption capacities up to 5.95 g g⁻¹ in I₂ solutions and 5.34 g g⁻¹ in I₃⁻ (KI/I₂) solutions.

Received 23rd January 2025,
Accepted 3rd April 2025

DOI: 10.1039/d5ma00061k

rsc.li/materials-advances

Introduction

Radioactive nuclides present an intricate challenge as they offer the advantage of producing clean nuclear energy with greenhouse-gas-free emissions, on the one hand, but they generate hazardous waste that poses substantial health and environmental risks if left untreated and released into the atmosphere, on the other hand.^{1,2} Among others, iodine nuclides are ominous byproducts resulting from plutonium-239 and uranium-235 fission in nuclear reactors; notably, iodine-129 is particularly dangerous due to its toxicity and extremely long half-life of ~16 million years, in addition to its capacity to easily pass through a wide variety of geological environments.^{3,4} Meanwhile, despite the much shorter half-life of iodine-131 estimated to be ~8 days, it poses an imminent threat to human health by disrupting metabolic processes through its severe radiation.⁵ Therefore, managing nuclear waste

is deemed crucial, especially when analyzing past nuclear accidents like Chernobyl in 1986 and Fukushima in 2011, where large amounts of radioactive iodine, including iodine-129 and iodine-131, were released into the atmosphere as gaseous iodine (I₂) or into water bodies as I₂ and I₃⁻.⁶ These incidents highlight the urgent need for advanced materials that can efficiently and rapidly capture and remediate iodine from various sources, namely, aqueous effluents.

Several materials have been identified as potent iodine adsorbents, including zeolites,⁷ ceramics,⁸ aerogels,^{9,10} metal–organic frameworks (MOFs),^{11–13} covalent organic frameworks (COFs),^{14,15} activated carbon (AC),¹⁶ and porous organic polymers.^{17,18} Nonporous materials have also demonstrated significant capture abilities.^{19,20} Among these, porous organic polymers have been of particular interest due to their prominent adsorption capacity, high physicochemical stability, lower synthesis costs, and robust linkages. In addition, organic polymers offer an on-demand structural flexibility depending on specific needs.²¹ It is noteworthy that there are several factors which depict the iodine capture by porous materials, such as their surface area and extended conjugation, and more importantly, the presence of binding sites and/or heteroatoms in the polymer's structure.^{22–25} Nevertheless, despite the high performance that these materials display in capturing gaseous iodine (I₂), most of them exhibit limited iodine uptake in aqueous environments, typically less than 1.0 g g⁻¹, namely because of their interference with water.^{26–30} Only a select few

^a Department of Mathematics and Natural Sciences, Gulf University for Science and Technology, Mubarak Al-Abdullah, Hawally 32093, Kuwait.

E-mail: alameddine.b@gust.edu.kw; Tel: +965 2530 7111

^b Functional Materials Group, Gulf University for Science and Technology, Mubarak Al-Abdullah, Hawally 32093, Kuwait

^c CSIR-Central Salt and Marine Chemicals Research Institute, Gijubhai Badheka Marg, Bhavnagar, Gujarat 364002, India

† Electronic supplementary information (ESI) available: Analysis of all compounds, and spectral data of NMR, FTIR, XPS, N₂ adsorption, TGA, kinetic studies, proposed I₂ adsorption mechanism and comparison of I₂ capture with different adsorbent materials. See DOI: <https://doi.org/10.1039/d5ma00061k>



materials have demonstrated a high iodine uptake capacity from water.^{31–35}

Iron(II) clathrochelate-based materials are exploited to a great extent across various applications owing to their structural modularity, exceptional chemical and physical stability, straightforward synthesis and ease of isolation, as well as their potential for post-functionalization.^{36–40} Various Fe(II) clathrochelate derivatives were synthesized and tested as adsorbents for different gases and dyes revealing astounding uptake capacities.^{41–46} Recently, our research group has developed a versatile synthetic methodology to make polyimide materials bearing Fe(II) clathrochelate as intercalators, portraying an impressive iodine vapor uptake of 680 wt%.⁴⁷ In this study, we report the synthesis of a series of three-dimensional polyarylamine copolymers incorporating iron(II) clathrochelate building blocks through a conventional Buchwald–Hartwig cross-coupling reaction. Iodine uptake tests reveal the exceptional adsorption properties of these 3D copolymers reaching 15 g g^{−1} in addition to the effective removal of iodine from aqueous and cyclohexane solutions revealing prominent capacities of 5.95 g g^{−1} and 1.11 g g^{−1}, respectively.

Experimental section

Synthesis

Synthesis of TAC1 (procedure A). The diamino Fe(II) clathrochelate monomer (DAC) was synthesized following a reported procedure.⁴⁷ In a microwave reactor, 1,3,5-tribromobenzene (0.15 g, 0.48 mmol, 1 equivalent) and DAC (0.49 g, 0.71 mmol, 1.5 equivalents) were dissolved in 9.5 mL of degassed DMF under a steady flow of argon. The reaction mixture was then supplemented with Pd₂(dba)₃ (0.036 g, 0.038 mmol, 8 mol%), XPhos (0.036 g, 0.076 mmol, 16 mol%), and sodium *tert*-butoxide (0.137 g, 1.43 mmol, 3 equivalents). The reaction was conducted under microwave irradiation at 180 °C for 2 hours under nitrogen. The resulting mixture was precipitated in methanol, filtered, and thoroughly washed with deionized water, methanol, acetone, dichloromethane (DCM), and petroleum ether. After drying under vacuum, a brown solid was obtained (330 mg, 92%). ¹³C-NMR (solid state, 125.8 MHz): δ 152.11, 133.82, 128.53, 116.43, 22.67 and 16.93. FTIR (KBr pellet, cm^{−1}): 3357 (N–H stretching), 2933 (aliphatic C–H stretching), 1591 (N–O stretching), 1488 (aliphatic C–H bending), 746 and 811 (aromatic C–H bending).

Synthesis of TAC2

TAC2 was synthesized using procedure A with tris(4-bromophenyl)amine (0.2 g, 0.41 mmol, 1 equivalent), DAC (0.43 g, 0.62 mmol, 1.5 equivalents), Pd₂(dba)₃ (0.03 g, 0.033 mmol, 8 mol%), XPhos (0.03 g, 0.066 mmol, 16 mol%), and sodium *tert*-butoxide (0.119 g, 1.24 mmol, 3 equivalents) dissolved in 8.3 mL of degassed DMF. The reaction yielded a brown solid (356 mg, 93%). ¹³C-NMR (solid state, 125.8 MHz): δ 153.33, 148.41, 136.51, 129.12, 124.88, 117.07, 25.45 and 20.17. FTIR (KBr pellet, cm^{−1}): 3333 (N–H stretching), 2935 (aliphatic C–H stretching), 1584 (N–O stretching), 1490 (aliphatic C–H bending), 770 and 810 (aromatic C–H bending).

Synthesis of TAC3

TAC3 was synthesized using procedure A with 1,3,5-tris(4-bromophenyl)benzene (0.2 g, 0.37 mmol, 1 equivalent), DAC (0.38 g, 0.55 mmol, 1.5 equivalents), Pd₂(dba)₃ (0.027 g, 0.029 mmol, 8 mol%), XPhos (0.027 g, 0.058 mmol, 16 mol%), and sodium *tert*-butoxide (0.106 g, 1.1 mmol, 3 equivalents) dissolved in 7.4 mL of degassed DMF. This reaction produced a brown solid (343 mg, 95%). ¹³C-NMR (solid state, 125.8 MHz): δ 155.21, 150.14, 136.55, 128.21, 122.33, 117.09, 112.71, 21.09 and 14.88. FTIR (KBr pellet, cm^{−1}): 3352 (N–H stretching), 2919 (aliphatic C–H stretching), 1591 (N–O stretching), 1488 (aliphatic C–H bending), 747 and 811 (aromatic C–H bending).

Iodine adsorption studies

The iodine vapor adsorption of TAC1–3 was analyzed using gravimetric techniques with 10 mg of each sample being used as an adsorbent by placing it in small weighing vials, which were then deposited in a larger vial to avoid any direct surface contamination during testing. The entire setup was tightly sealed in a container having iodine pellets at its bottom and the temperature was maintained at 353 K to promote adsorption. At various time intervals, the vials with the adsorbents were weighed and the percentage of I₂ uptake was calculated using the following formula:

$$\text{Iodine uptake} = \frac{(w_2 - w_1)}{w_1} \times 100 \text{ wt\%} \quad (100 \text{ wt\%} \equiv 1 \text{ g g}^{-1}) \quad (1)$$

where w_1 and w_2 denote the masses of the copolymer before and after iodine adsorption, respectively.

Kinetics and adsorption equilibrium of iodine

The kinetics of iodine adsorption were quantitatively analyzed using the pseudo-1st-order, pseudo-2nd-order, and intra-particle diffusion models as represented by eqn (2)–(4), respectively:

$$\ln(q_e - q_t) = \ln q_e - k_1 t \quad (2)$$

$$\frac{t}{q_t} = \frac{t}{q_e} + 1/k_2 \quad (3)$$

$$q_t = k_p t^{0.5} + C \quad (4)$$

where q_t (mg g^{−1}) and q_e (mg g^{−1}) represent the amount of iodine adsorbed per gram of adsorbent at time t and at equilibrium, respectively. The rate constants for the pseudo-1st-order, pseudo-2nd-order, and intra-particle diffusion models are denoted by k_1 , k_2 and k_p , respectively.^{48,49}

Iodine uptake capability from cyclohexane

A 20 mL cyclohexane solution containing 100 mg L^{−1} of iodine was introduced to a 10 mg sample of TAC1–3, placed in a tightly closed glass vial, and kept in the dark for 24 hours. Subsequently, 2 mL of the supernatant was extracted and transferred into a quartz cuvette to measure its absorbance and determine the iodine concentration. This procedure was repeated for each polymer using cyclohexane solutions with iodine concentrations of 300 mg L^{−1}, 500 mg L^{−1} and 1000 mg L^{−1}. The iodine uptake by the TAC1–3 samples was calculated using the



following formula:

$$q_t = \frac{(C_0 - C_t)V}{m} \quad (5)$$

In this formula, V represents the volume of the iodine-cyclohexane solution (L), m is the mass of the **TAC1-3** sample (g), and C_0 is the initial iodine concentration in the cyclohexane solution (mg L^{-1}). The iodine concentration in cyclohexane after 24 hours of adsorption is denoted as C_t .⁵

The following formula is used to calculate the efficiency of iodine removal by the **TAC1-3** samples:

$$W = \frac{C_0 - C_t}{C_0} \times 100\% \quad (6)$$

where C_0 represents the initial iodine concentration in cyclohexane, while C_t denotes the iodine concentration after 24 hours of adsorption.⁵⁰

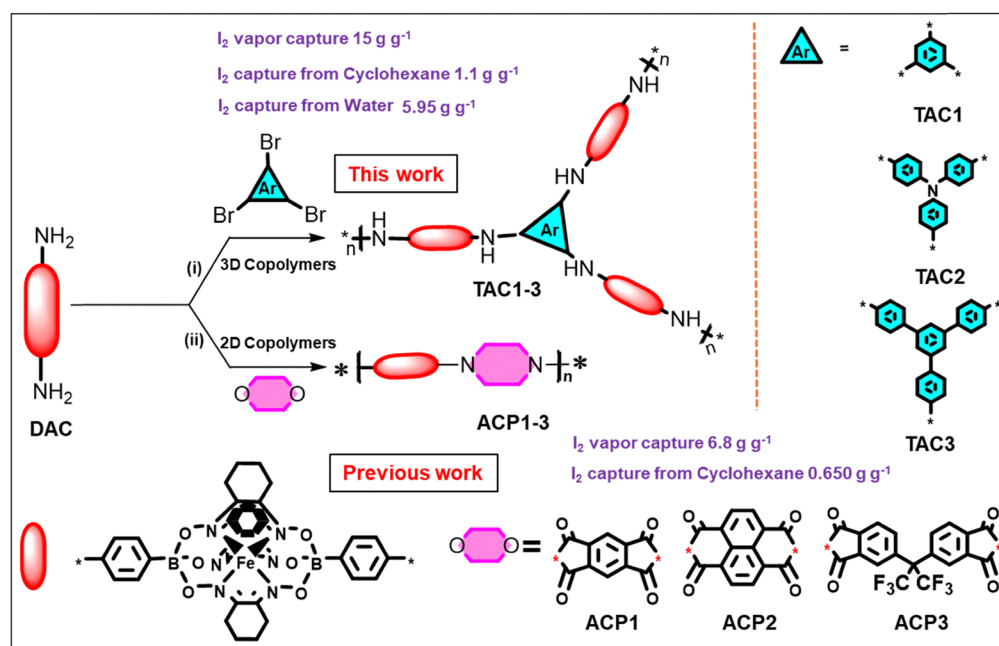
Iodine uptake capacity from water

TAC1-3 samples were immersed in an aqueous iodine solution, either containing I_2 (3 mg of adsorbent in 100 mL of 1 mM solution) or I_3^- (5 mg of adsorbent in a solution of 300 mg KI and 150 mg I_2 in 100 mL of water). The solution was analyzed using UV-Vis spectroscopy, and the iodine absorbed by the **TAC1-3** samples was calculated using eqn (5), where V represents the volume of the aqueous iodine solution (L), m is the mass of the **TAC1-3** sample (g), and C_0 (g L^{-1}) and C_t (g L^{-1}) are the iodine concentrations in the solution before and after adsorption, respectively.

Results and discussion

It is worthwhile to mention that while our current work employed the previously reported diamino iron(II) clathrochelate building block, **DAC**,⁴⁷ the latter was utilized as a surrogate for the preparation of clathrochelate-based imide copolymers (**ACP1-3**) through a cyclocondensation reaction under microwave heating, as illustrated in Scheme 1. Copolymers **ACP1-3** have demonstrated remarkable iodine vapor uptake of 6.8 g g^{-1} and exhibited an uptake of up to 0.65 g g^{-1} in cyclohexane solution. These exceptional iodine adsorption capacities prompted us to design new copolymers bearing **DAC** with the prospect of enhancing iodine adsorption through the incorporating of secondary amino groups into the polymer backbone. It is noteworthy that in previous work, we synthesized linear secondary arylamine copolymers containing iron(II) clathrochelate units **CLP1-3**³⁸ before we had modified them into tertiary arylamine derivatives **PCLP1-3** using a Buchwald-Hartwig cross-coupling reaction. Therefore, this motivated us to develop three-dimensional secondary arylamine copolymers as potential adsorbents of iodine.

In the current work secondary arylamine copolymers containing clathrochelate units, **TAC1-3**, were synthesized *via* a Buchwald-Hartwig amination cross-coupling reaction, which was performed in DMF at 180°C for 2 hours under microwave heating, utilizing the diamine iron(II) clathrochelate synthon (**DAC**) in combination with different tribrominated aryl derivatives, including 1,3,5-tribromobenzene, tris(4-bromophenyl)amine, and 1,3,5-tris(4-bromophenyl)benzene, as shown in Scheme 1. The resulting copolymers were obtained in excellent yields and were purified using simple filtration followed by extensive washing of the solid with



Reaction conditions: (i) $\text{Pd}_2(\text{dba})_3$, Xphos, NaOtBu , DMF, MW, 180°C , 2h; (ii) imidazole, DMF, MW, 180°C , 2h.

Scheme 1 Synthesis of copolymers **TAC1-3** and comparison with the previous work **ACP1-3**. Reaction conditions: (i) $\text{Pd}_2(\text{dba})_3$, Xphos, NaOtBu , DMF, MW, 180°C , 2 h; (ii) imidazole, DMF, MW, 180°C , 2 h.

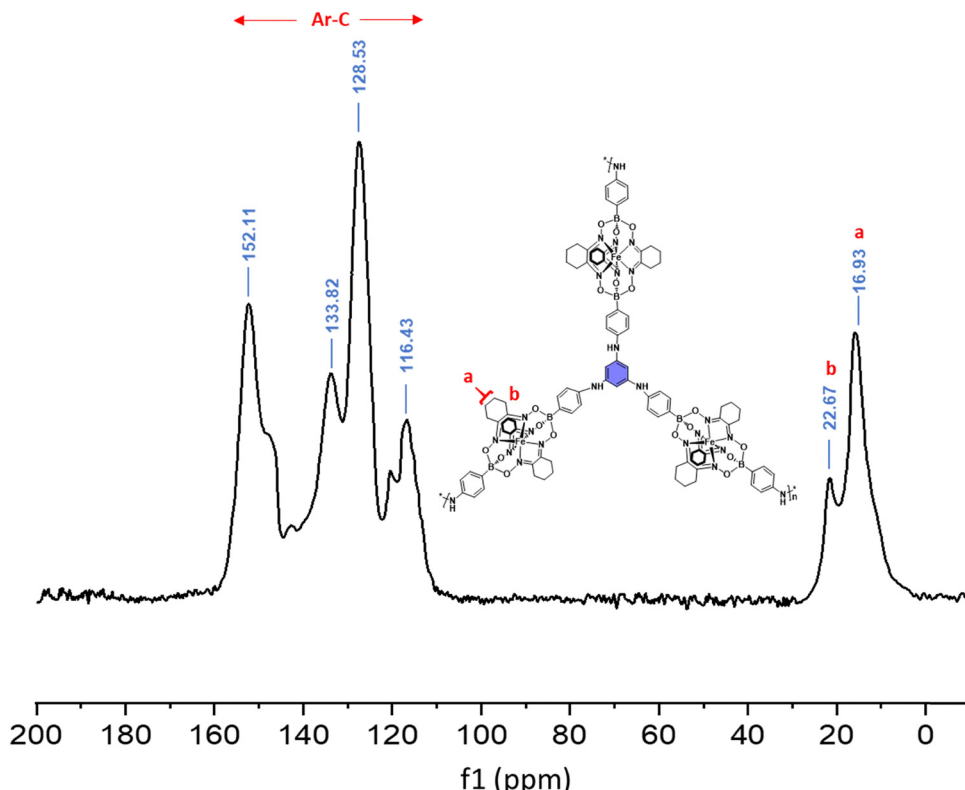


Fig. 1 ^{13}C -NMR spectrum (solid-state) of **TAC1**.

demineralized water, acetone, methanol (MeOH), dichloromethane, and naphtha (petroleum ether). The copolymers **TAC1-3** were found to be insoluble in various organic solvents, such as dimethylformamide (DMF), DCM, chloroform, THF, and methanol. Consequently, the formation and purity of the target copolymers were confirmed by carrying out a careful structural analysis using various solid-state techniques, such as ^{13}C -NMR spectroscopy, Fourier-transform infrared spectroscopy (FTIR), and X-ray photoelectron spectroscopy (XPS) (see Fig. 1–3 and Fig. S1–S7 in the ESI[†]).

Fig. 1 represents the ^{13}C -NMR spectrum (solid-state) of the target copolymer **TAC1**, clearly displaying all the expected peaks. The peaks between 152.11 ppm to 116.43 ppm correspond to the aromatic (sp^2) carbons while the signals at 22.67 ppm and 16.93 ppm (Fig. 1, peaks a and b) are fingerprints of aliphatic sp^3 carbon atoms of the cyclohexyl groups present in the clathrochelate unit. Similarly, the solid-state ^{13}C -NMR spectra of **TAC2** and **TAC3** display similar distinct chemical shifts, as can be noticed in Fig. S1 and S2 of the ESI[†].

As illustrated in Fig. 2, the relative FT-IR absorption spectra of the two precursor materials **TBB** and **DAC** compared to the target copolymer **TAC3** exhibit all the expected differences between the peaks of the starting materials and target compound, thus confirming the successful synthesis of the latter. The N–H stretching vibrations observed in **DAC** at 3412 cm^{-1} are shifted to 3352 cm^{-1} along with a noticeable decrease in the peak intensity in **TAC3**, which confirms the formation of the secondary amine copolymers.⁵¹ On the other hand, the

fingerprint C–Br stretching vibrations observed in **TBB** at 695 cm^{-1} disappeared in the **TAC3** spectrum, signifying the total consumption of all the reactants, and confirming the successful formation of the copolymers.⁵² Additionally, **TAC3** reveals other distinctive aromatic C–H vibrations at 3032 cm^{-1} (stretching), and at 811 cm^{-1} and 747 cm^{-1} (vibrations).⁵³ Furthermore, the characteristic frequencies of the aliphatic C–H groups are observed at 2919 cm^{-1} (str) and 1488 cm^{-1} (ben).⁵⁴ Likewise, the absorption band at 1591 cm^{-1} is attributed to the stretching frequency of the N–O groups,⁵⁵ supporting further evidence of the effective formation of **TAC3**. It is also worth mentioning that both **TAC1** and **TAC2** display their distinctive FT-IR peaks, proving their efficacious formation as well (Fig. S3 and S4 in the ESI[†]).

Survey-scan X-ray photoelectron spectroscopy (XPS) data of **TAC1-3** corroborate the existence of the desired elements. The binding energies for C 1s, O 1s, and N 1s were determined to range between $284.4\text{--}284.7\text{ eV}$, $531.9\text{--}532.2\text{ eV}$, and $399.3\text{--}399.4\text{ eV}$, correspondingly. Meanwhile, the B 1s and Fe 2p binding energies were observed in the range of $190.6\text{--}190.7\text{ eV}$ and $709.1\text{--}722.1\text{ eV}$, respectively⁵⁶ (Fig. 3 and Fig. S6, S7 in the ESI[†]).

BET surface area studies

The microporous nature of **TAC1-3** was examined at low relative pressure using N_2 adsorption tests conducted at 77 K (Fig. S8 in the ESI[†]). The surface areas and pore volumes of the target copolymers were determined from the Brunauer–Emmett–Teller



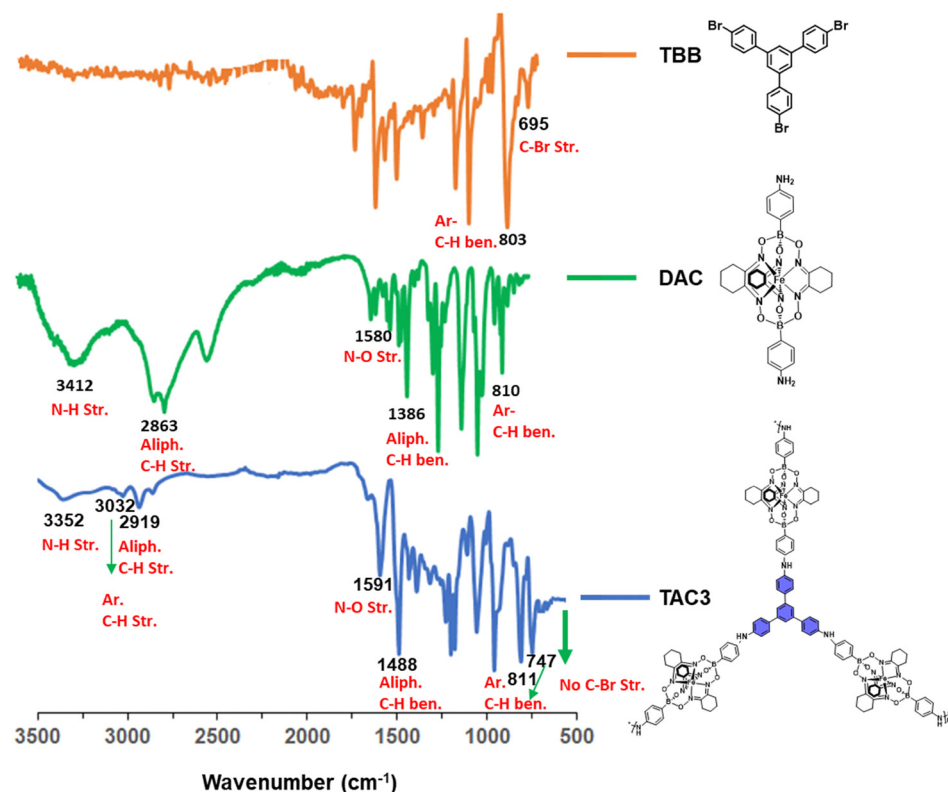


Fig. 2 FT-IR spectra of TBB (up), DAC (middle) and TAC3 (down).

(BET) theory based on the obtained isotherms. TAC1–3 demonstrated BET surface areas of up to 69 m² g⁻¹ and pore volumes

ranging from 0.096 cm³ g⁻¹ to 0.6 cm³ g⁻¹ (Table S1 in the ESI[†]). The limited BET surface areas of TAC1–3 can be attributed to

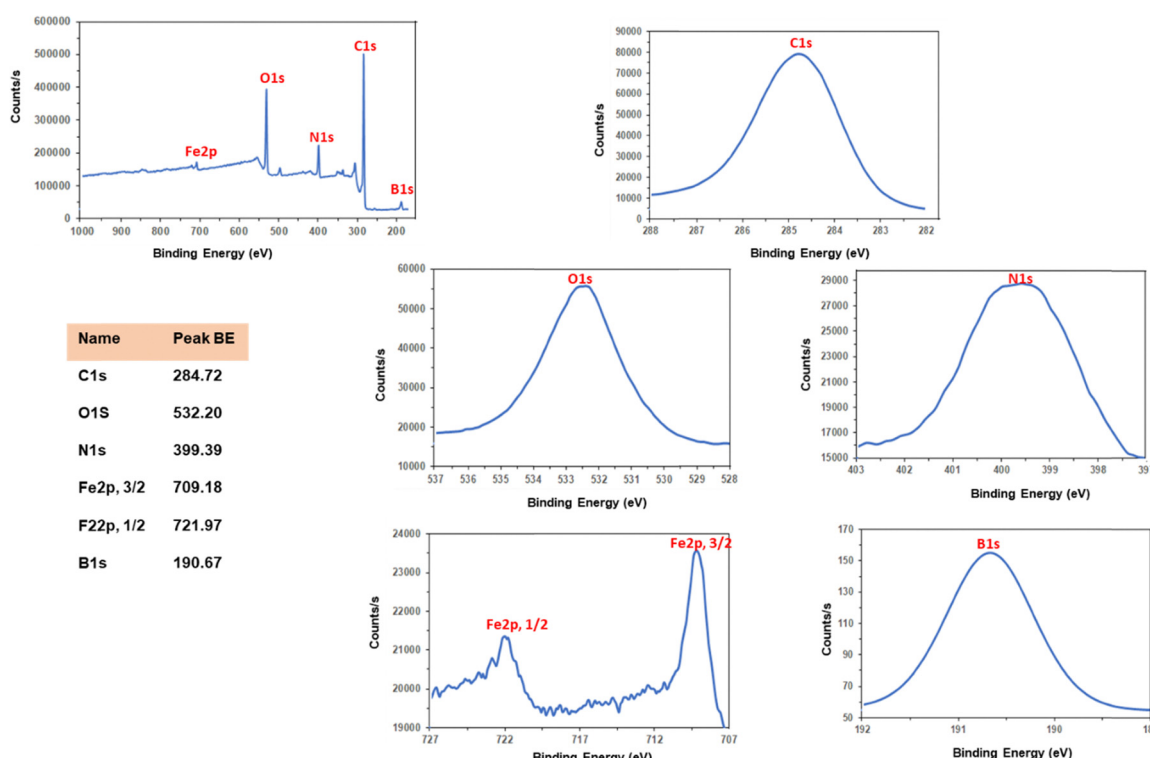


Fig. 3 XPS spectrum of TAC1.

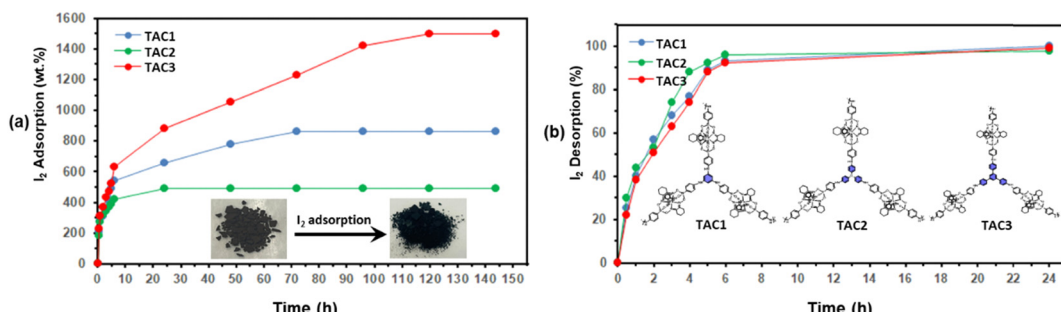


Fig. 4 Weight percentage (wt%) of iodine (I_2) vapor capture (a) (inset: sample images showing a color change from brown to black due to iodine adsorption prior and subsequently) and release (b) by **TAC1-3**.

kinetic restrictions at the cryogenic temperature of 77 K, which impede molecular nitrogen diffusion into the micropores.^{47,57}

Iodine capture

Experimental gravimetric tests were carried out to investigate the iodine vapor adsorption characteristics of **TAC1-3**. These studies involved exposing a 10 mg sample of a particular copolymer to excess $I_2(s)$ in a sealed container at 353 K under atmospheric pressure. The amount of adsorbed iodine was monitored at different intervals until saturation was reached (Fig. 4). The results disclosed remarkable iodine uptakes, namely for **TAC3**, which achieved an adsorption capacity of 1500 wt% (15 g g⁻¹) after 5 days of exposure (Table 1 and Fig. 4). This exceptionally high iodine vapor absorption underscores **TAC3** as a prominent adsorbent, especially considering its comparatively easy and adaptable production in comparison to other materials documented in the literature (Table S2, ESI[†]).^{23,57-66} Both **TAC1** and **TAC2** displayed very good iodine capture capacities of 860 wt% and 490 wt%, respectively. The extraordinary iodine adsorption values observed in **TAC1-3**, ranging from 490 to 1500 wt%, are attributed to the complex structural properties of the copolymers featuring numerous adsorption sites,^{31,47,67,68} which allows for an efficient iodine capture capacity that is not only influenced by the copolymers' specific surface areas but also the existence of binding sites. Moreover, the presence of terphenyl groups, which are known to enhance the aromatic π interactions with iodine,⁶⁹ in the **TAC3** copolymer's skeleton boosts its iodine capacity when compared to **TAC1** and **TAC2**.

As it can be perceived from the comparative thermograms for the iodine-loaded samples, designated as **TAC1-3@I₂**, and those for the pure copolymers, there is a clear decline in the 10% weight loss temperatures in the range of 125–134 °C for

the iodine-bearing copolymers from the initial 288–335 °C temperature values recorded for the **TAC1-3** (Fig. S9 and S10 in the ESI[†]).^{70,71} Furthermore, FTIR spectroscopy was utilized to analyze the characteristics of **TAC1-3@I₂**, which were found to exhibit conspicuous variations in their vibrational bands when compared to their pure counterparts **TAC1-3**. As shown in Fig. 5, the FTIR spectrum of **TAC3@I₂** displays significant shifts attributed to iodine adsorption, particularly in the aliphatic C-H stretching ($\sim 14\text{ cm}^{-1}$) and bending bands ($\sim 5\text{ cm}^{-1}$), as well as the aromatic C-H stretching ($\sim 68\text{ cm}^{-1}$) and bending bands ($\sim 31\text{ cm}^{-1}$). Additionally, notable shifts are observed in the stretching frequencies of the functional groups such as N-H ($\sim 50\text{ cm}^{-1}$) and N-O ($\sim 6\text{ cm}^{-1}$) in the iodine adsorbed copolymer **TAC3@I₂**. These changes strongly indicate interactions between the hitherto mentioned copolymer and iodine molecules, especially involving the aromatic rings, amine groups, and N-O units. These aforementioned binding interaction sites which contain electron lone pairs can effectively interact with iodine to form polyiodide anions, thus resulting in the observed shifts in the corresponding groups^{68,72} (Fig. S14 in the ESI[†]). Furthermore, the electrostatic potential of the amino groups decreases the conjugation with the aromatic rings, which enhances their interaction with iodine molecules, consequently, further improving their I_2 absorption capacity.⁷³ It is noteworthy that the observed FTIR peak shifts confirm the presence of weak interactions between the copolymers and I_2 , indicating a physisorption behavior which occurs at the surface of **TAC1-3**.⁷⁴

To gain more insight into the adsorption of iodine species by **TAC1-3**, XPS analysis was performed after iodine adsorption and the spectra were compared to those prior to adsorption (Fig. 6 and Fig. S11, S12 in the ESI[†]). The XPS survey scan spectrum of **TAC3** (Fig. 6) lacks the characteristic binding energy peaks corresponding to iodine's 3d orbital, whereas that of **I₂@TAC3** discloses the effective adsorption of iodine moieties, as evidenced by the existence of iodine 3d orbital signals in the range of 619–634 eV.^{75,76} Two pronounced peaks, ascribed to the $I_{3d,3/2}$ and $I_{3d,5/2}$ energy levels, were also observed at 632.58 eV and 621.02 eV, respectively. Additionally, the appearance of two more peaks alongside the $I_{3d,3/2}$ and $I_{3d,5/2}$ peaks represents the manifestation of polyiodide species (I^- and I^{3-}) along with molecular iodine (I_2).⁷⁷ Furthermore, the slight shifts in the binding energies of all the copolymers' constituting elements

Table 1 Overview of I_2 vapor sorption capabilities by copolymers **TAC1-3**

Entry	Copolymer	wt% I_2 capture	% I_2 release ^a
1	TAC1	860 ^b	100
2	TAC2	490 ^a	98
3	TAC3	1500 ^c	99

Maximum capacity was reached. ^a After 1 day. ^b After 2 days. ^c After 5 days.



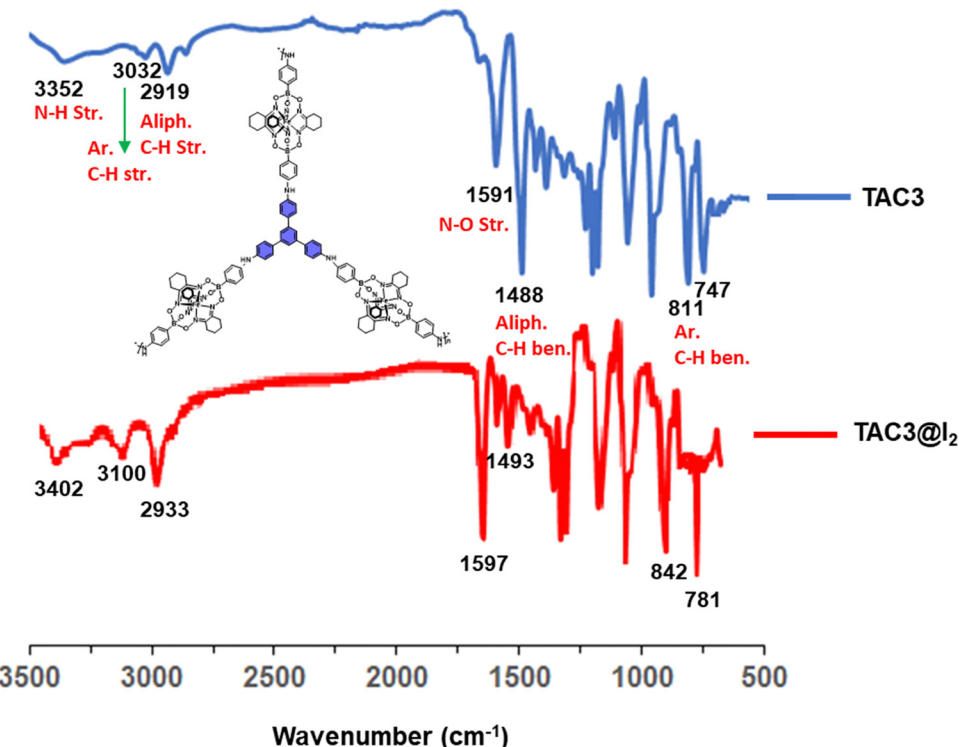


Fig. 5 FTIR spectra of **TAC3** (top) and **TAC3@I₂** (bottom).

after iodine adsorption suggest that the adsorption affinity of the latter is prompted not only by the copolymers' surface areas but also by the presence of active binding sites.³¹

Experimental tests were conducted to investigate the mechanism of iodine adsorption by TAC1-3 through kinetic studies using pseudo-1st-order, pseudo-2nd-order, and intra-particle diffusion models, as outlined in eqn (2)-(4). Fig. 7 presents the calculated equilibrium uptake capacity ($q_{e,cal}$) for the pseudo-1st-order model, obtained by plotting $\ln(q_e - q_t)$ against time (t). Conversely, the $q_{e,cal}$ values for the pseudo-2nd-order

model were determined by plotting t/q_t vs. time (t) for **TAC3**. Table 2 summarizes the iodine adsorption data for **TAC3** based on both models, clearly showing a higher correlation coefficient (R^2) of 0.9784 for the pseudo-2nd-order model, compared to 0.9595 for the pseudo-1st-order model. The correlation coefficient obtained from the intra-particle diffusion model for **TAC3** ($R^2 = 0.9595$) appears to be lower than that of the pseudo-2nd-order kinetic model (Fig. S15 in the ESI[†]). This clearly indicates a better fit of the experimental data with the pseudo-2nd-order model, especially when the experimental

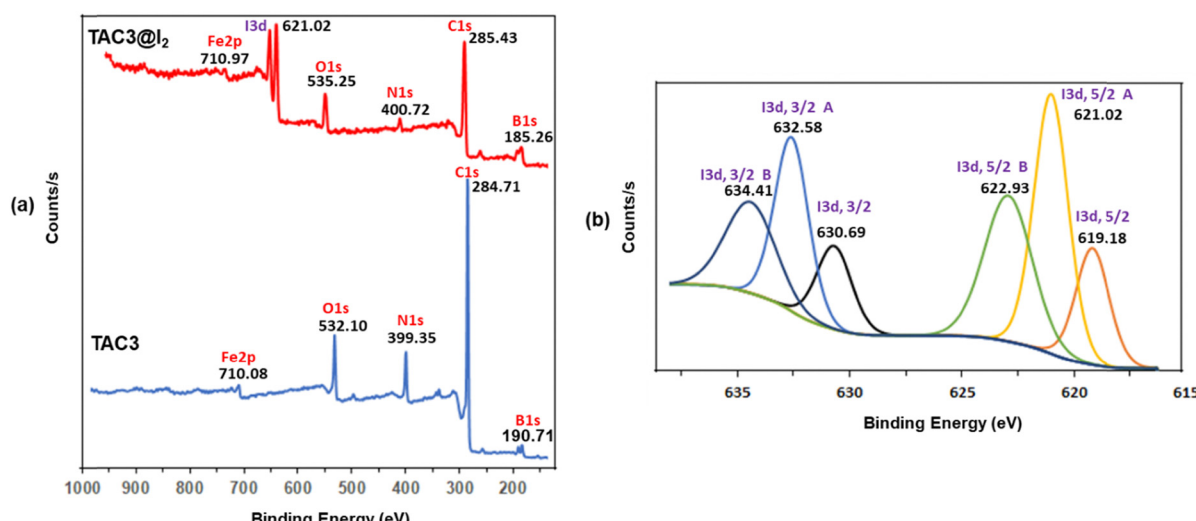


Fig. 6 XPS analysis spectra of **TAC3** prior and post iodine capture (a) and high resolution (HR)-XPS spectra of I3d of **TAC3@I₂** (b).



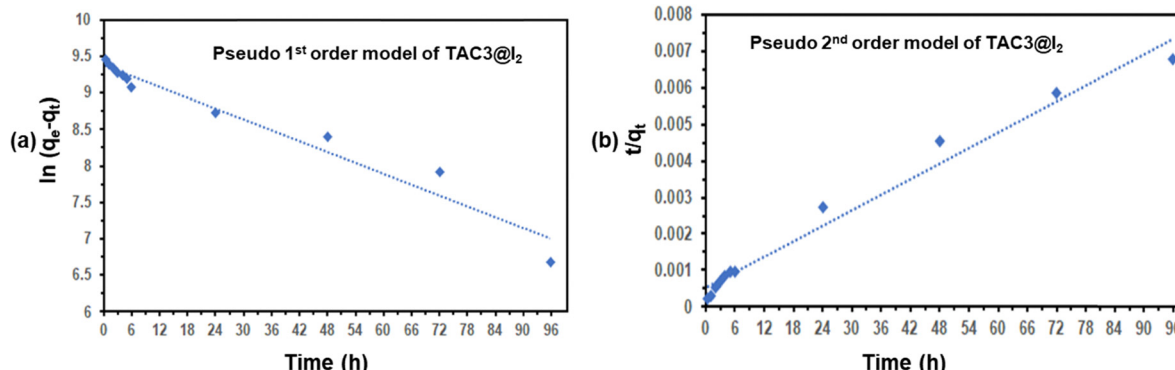


Fig. 7 Kinetic studies of **TAC3@I₂**: (a) pseudo 1st order and (b) pseudo 2nd order models.

iodine adsorption capacity at equilibrium ($q_{e,exp}$) of 15 g g⁻¹ is benchmarked against the calculated value ($q_{e,cal}$) of 14.3 g g⁻¹ from the pseudo-2nd-order model. These results strongly suggest that iodine adsorption by TAC3 follows a pseudo-2nd-order kinetic model. Likewise, the other copolymers, **TAC1** and **TAC2**, were also found to conform to the pseudo-2nd-order kinetic model (Table 2 and Fig. S13–S15 in the ESI†). This finding proposes an adsorption behavior that is strongly influenced by the prerequisite for the adsorbate and adsorbent-free sites to interact in order for the uptake to take place, thus leading to a relatively longer time for the process, which affects the iodine sorption overall rate.⁷⁸

Desorption trials were made by exposing the iodine-loaded copolymers **TAC1–3@I₂** to heat (120 °C), as shown in Fig. 4 and outlined in Table 1. This method lead to the release of ~98% of the captured iodine in the very first 6 hours followed by achieving quantitative desorption after 24 hours of continuous heating. Further investigation into iodine desorption was conducted by immersing the **TAC3@I₂** copolymer in ethanol (EtOH), a well-known solvent of I₂, which released the latter from **TAC3@I₂** as proven from the UV-Vis spectra recorded for ethanolic solution at various time periods (Fig. 8).⁷⁹ Most of the adsorbed iodine was released in the ethanol medium during the first 40 minutes of immersion followed by a slower release

Table 2 Summary of the kinetic parameters for **TAC1–3@I₂**

Polymer	Pseudo 1st order model			R^2	Pseudo 2nd order model		
	$q_{e,exp}$ (g g ⁻¹)	$q_{e,cal}$ (g g ⁻¹)	k_1 (h ⁻¹)		$q_{e,cal}$ (g g ⁻¹)	k_2 (h ⁻¹)	R^2
TAC1@I₂	8.6	5.4	-5.7×10^{-4}	9.49×10^{-1}	8.3	1.4×10^{-4}	9.93×10^{-1}
TAC2@I₂	4.9	3.1	-9.9×10^{-3}	9.69×10^{-1}	5.0	2.0×10^{-4}	9.93×10^{-1}
TAC3@I₂	15	11.8	-2.0×10^{-4}	9.59×10^{-1}	14.3	9.8×10^{-6}	9.78×10^{-1}

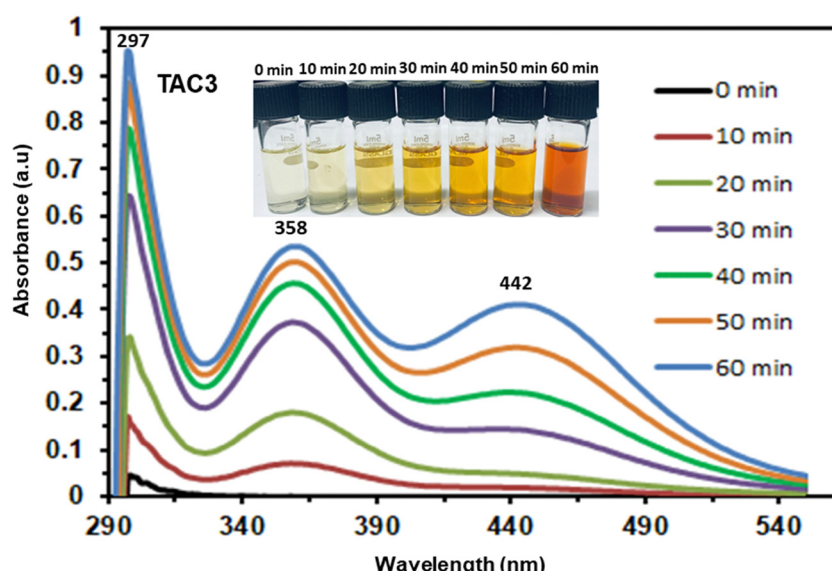


Fig. 8 UV-Vis absorption graph of iodine release from **TAC3@I₂** in ethanol.



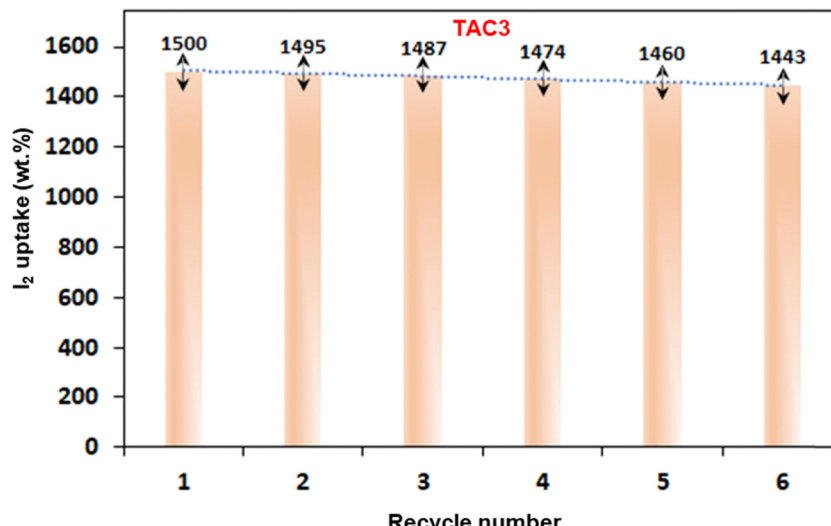


Fig. 9 Iodine capture reuse efficiency of TAC3.

rate attaining equilibrium after 1 hour. These results emphasize the ease with which TAC3 can be regenerated, either by heating or immersion in ethanol, hence underscoring its potential usage as a renewable material.

Investigation of TAC3 regeneration was examined by heating the copolymer **TAC3@I₂** to 120 °C for one day to completely release the captured iodine and isolate the regenerated copolymer **TAC3(R)**, which was subsequently exposed to iodine vapors before measuring its uptake capacity employing the previously

described gravimetric method. This capture-release cyclic procedure was repeated using the same copolymer sample for six consecutive times showing only a minor drop of 3.8%, which has proven the sturdy iodine capacity of TAC3 (Fig. 9).

The iodine adsorption efficiency of copolymers **TAC1–3** in cyclohexane mixtures was studied at various dilutions (100 mg L⁻¹, 300 mg L⁻¹, 500 mg L⁻¹ and 1000 mg L⁻¹) during 24 hours (Fig. 10, 11, and Fig. S16 in the ESI[†]). The mother liquors' absorbance was monitored with a UV spectrophotometer, to

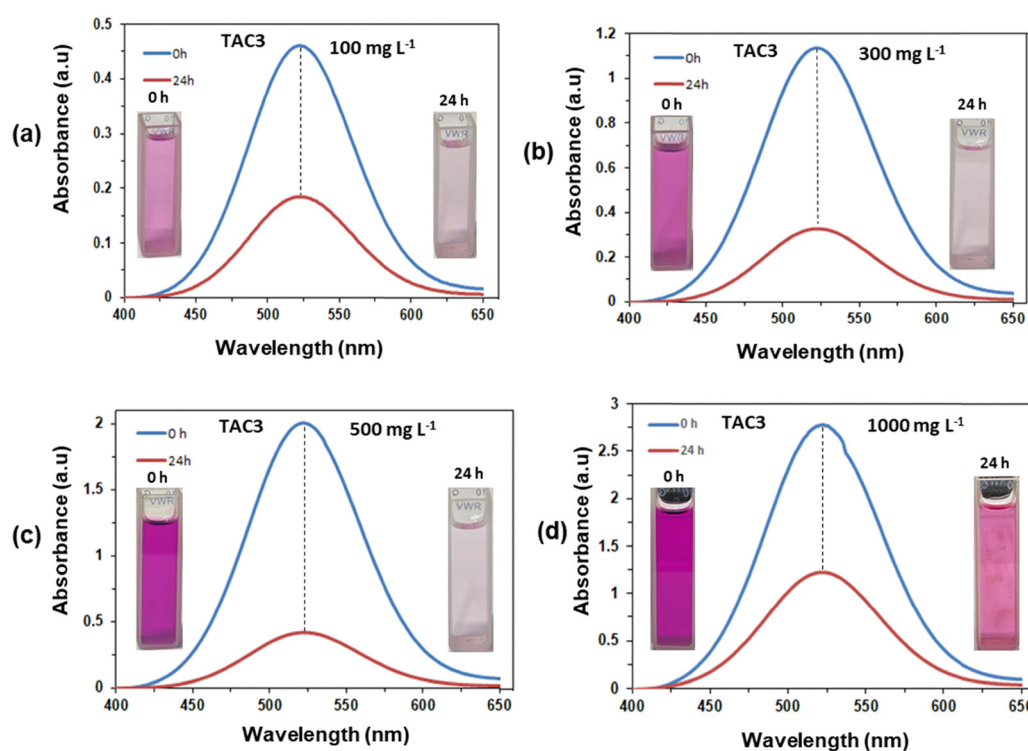


Fig. 10 UV-Vis absorption spectra of **TAC3** were recorded after exposing it to iodine concentrations of 100 mg L⁻¹ (a), 300 mg L⁻¹ (b), 500 mg L⁻¹ (c) and 1000 mg L⁻¹ (d) in cyclohexane solution for 24 hours.



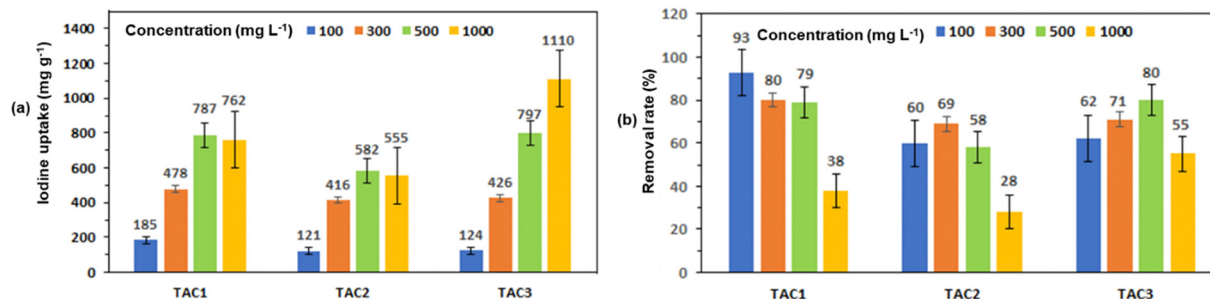


Fig. 11 The amount of iodine adsorbed (a) and removed (b) by **TAC1–3** from cyclohexane solutions with various iodine concentrations.

Table 3 Adsorption and removal rates of **TAC1**, **TAC2**, and **TAC3** from cyclohexane

Polymer	Initial concentration (mg L⁻¹)	Adsorption capacity (mg g⁻¹)	Removal efficiency (%)
TAC1	100	185	93
	300	478	80
	500	787	79
	1000	762	38
TAC2	100	121	60
	300	416	69
	500	582	58
	1000	555	28
TAC3	100	124	62
	300	426	71
	500	797	80
	1000	1110	55

determine the amount of iodine absorbed by **TAC1–3** against a standardized absorption spectrum, as shown in Fig. 10(a)–(d).

Table 4 Summary of I_2 sorption capacities from aqueous solution by **TAC1–3**

Entry	Polymer	I_2 adsorption after 24 h (g g⁻¹)
1	TAC1	4.85
2	TAC2	4.58
3	TAC3	5.95

Fig. 11(a) depicts the quantity of iodine adsorbed for **TAC1**, **TAC2**, and **TAC3** from 100 mg L^{-1} iodine in cyclohexane preliminary concentration, revealing uptake capacities of 185 mg g^{-1} , 121 mg g^{-1} , and 124 mg g^{-1} , respectively. When testing the copolymers' iodine adsorption capacity from 300 mg L^{-1} of I_2 in cyclohexane, the adsorbed amounts were found to be 478 mg g^{-1} , 416 mg g^{-1} , and 426 mg g^{-1} for **TAC1**, **TAC2**, and **TAC3**, respectively. Similarly, when using an initial concentration of 500 mg L^{-1} , the adsorption amounts were 787 mg g^{-1} , 582 mg g^{-1} , and 797 mg g^{-1} for **TAC1**, **TAC2**, and **TAC3**, respectively.

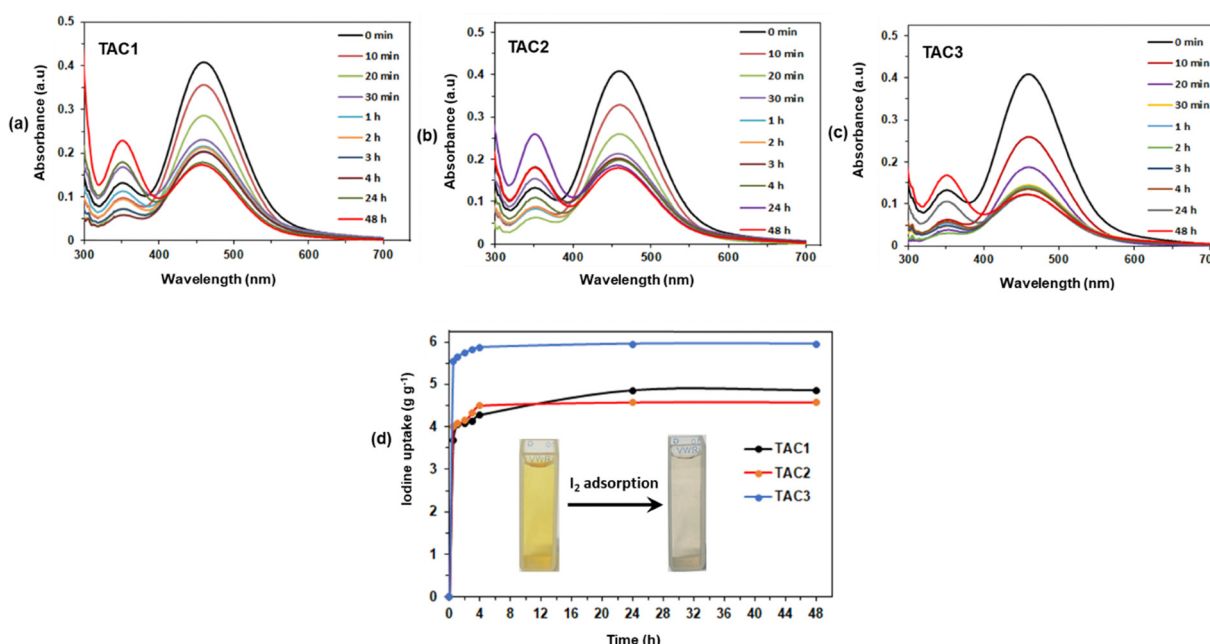


Fig. 12 UV-Vis absorption spectra of an aqueous solution of iodine (1 mM) upon adding **TAC1** (a), **TAC2** (b) and **TAC3** (c). Maximum I_2 adsorption capacity measurements for all three copolymers **TAC1–3** (d) (inset: images showing the color change of aqueous I_2 solutions before and after adsorption by **TACs**).



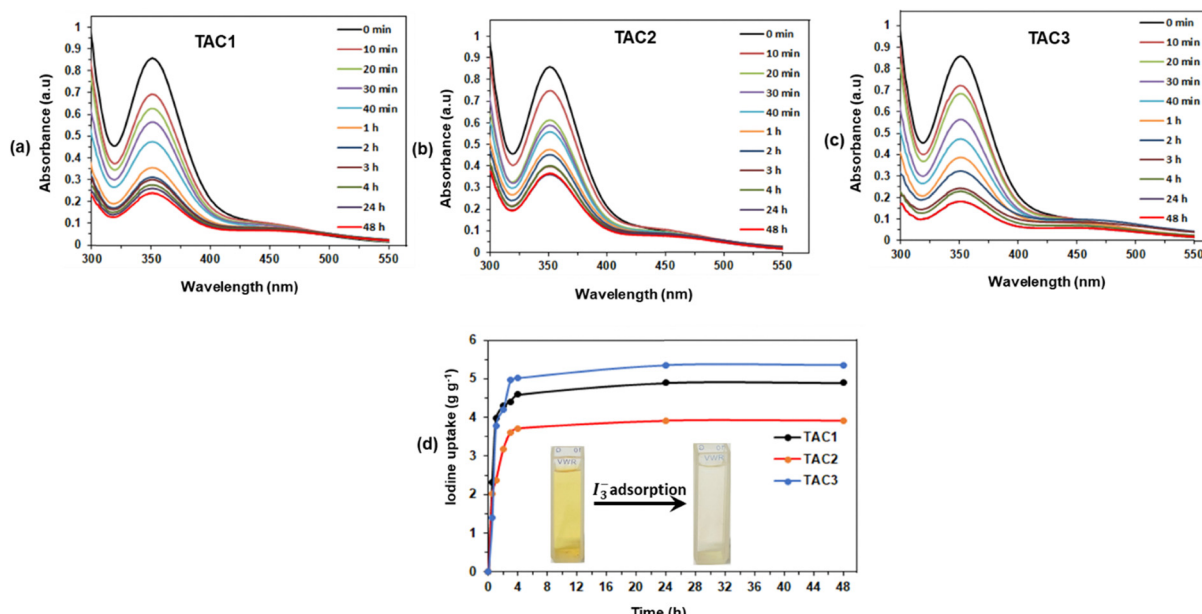


Fig. 13 UV-Vis absorption spectra of iodine adsorption from aqueous I_3^- solution upon adding **TAC1** (a), **TAC2** (b) and **TAC3** (c). Maximum I_3^- adsorption capacity measurements for **TAC1–3** (d) (inset: images showing the color change of aqueous I_3^- solutions before and after adsorption by **TACs**).

Furthermore, when using a solution with an initial concentration of 1000 mg L^{-1} , the adsorption amounts were found to be 762 mg g^{-1} , 555 mg g^{-1} , and 1110 mg g^{-1} for **TAC1**, **TAC2**, and **TAC3**, respectively. Fig. 11(b) illustrates the iodine elimination efficacy of **TAC** samples in the different iodine in cyclohexane solutions (*i.e.*, 100 mg L^{-1} , 300 mg L^{-1} , 500 mg L^{-1} and 1000 mg L^{-1}), where **TAC1** exhibited removal efficiencies of 93%, 80%, 79% and 38% at different dilutions, whereas **TAC2** portrayed efficiencies of 60%, 69%, 58% and 28%. Likewise, **TAC3** displayed exclusion efficiencies of 62%, 71%, 80% and 55% for iodine in cyclohexane solutions whose concentrations ranged from 100 mg L^{-1} to 1000 mg L^{-1} , as shown in Table 3. The differences in iodine adsorption and removal rates among **TAC1**, **TAC2**, and **TAC3** can be attributed to their structural properties, the distribution of active sites, and the initial iodine concentration. **TAC3** appears to be the most efficient polymer for iodine adsorption from cyclohexane solutions, especially at higher concentrations, due to its superior structural characteristics and higher number of active sites. However, beyond 1000 mg L^{-1} concentrations, the removal efficiency of **TAC3** drops significantly, indicating saturation of the active sites.^{22,80} **TAC3** showed the maximum iodine uptake capacity of 1110 mg g^{-1} at a concentration of 1000 mg L^{-1} (Fig. 11(a)), which highlights the copolymer's exceptional ability to remove iodine from cyclohexane solutions, surpassing other adsorptive materials reported in the literature (Table S3, ESI[†]).^{15,81–85}

The remarkable iodine adsorption performance of **TAC1–3** from the vapor phase and cyclohexane prompted testing their ability to capture I_2 from aqueous media. Therefore, the copolymers were added to 1 mM solutions of iodine in water and their uptake capacities were measured by UV/Vis spectroscopic analysis (Fig. 12a–c), which revealed efficient iodine adsorption within the first 30 minutes. It is worthwhile to note that the

aqueous solution color changed from dark yellow to colorless (inset of Fig. 12d). The iodine uptake reached equilibrium within 24 hours and the maximum I_2 uptake capacities recorded for **TAC1**, **TAC2**, and **TAC3** were found to be 4.85 g g^{-1} , 4.58 g g^{-1} , and 5.95 g g^{-1} , respectively (Table 4 and Fig. 12). This exceptional iodine (I_2) adsorption from aqueous solution for **TAC3** is very promising, especially when benchmarked against other adsorbents reported in the literature (Table S4, ESI[†]).^{29,68,86–88}

In addition to neutral I_2 , both iodide (I^-) and triiodide (I_3^-) are two significant anionic iodine species. In aqueous media, I_2 tends to form triiodide (I_3^-) species by the dynamic equilibrium $I_2 + I^- \rightleftharpoons I_3^-$, especially when I^- is present. Therefore, the adsorption of triiodide is crucial for effective iodine remediation. To evaluate the effectiveness of the copolymers **TAC1–3** in adsorbing I_3^- (also referred to as I_2/I^-), adsorption experiments were conducted by immersing the copolymers in a KI_3 solution, which was prepared by dissolving 300 mg KI and 150 mg I_2 in 100 mL of water, for 48 hours and the iodine removal was monitored by UV-Vis spectroscopy (Fig. 13a–c). Interestingly, the iodine uptake capacities were found to be 4.89 g g^{-1} for **TAC1**, 3.90 g g^{-1} for **TAC2**, and 5.34 g g^{-1} for **TAC3** (Table 5 and Fig. 13d). These results demonstrate the exceptional ability of copolymers **TAC1–3** to adsorb I_3^- from aqueous media, surpassing the performance of other materials reported in the literature (Table S5, ESI[†]).^{89–94}

Table 5 Summary of I_3^- sorption capacities from aqueous solution by **TAC1–3**

Entry	Copolymer	I_3^- adsorption after 24 h (g g^{-1})
1	TAC1	4.89
2	TAC2	3.90
3	TAC3	5.34



Conclusion

In summary, we have successfully synthesized a novel class of 3D metal-organic copolymers, **TAC1-3**, featuring Fe(II) clathrochelate units with various secondary arylamine linkages, demonstrating strong potential for sustainable applications. Iodine gas adsorption findings revealed an impressive sorption capacity of 1500 wt% and conformed to a pseudo-2nd-order kinetic model. Additionally, these copolymers demonstrated significant iodine uptake in cyclohexane, achieving an extreme adsorption capacity of 1.11 g g^{-1} at an initial iodine concentration of 1000 mg L^{-1} . Regeneration tests confirmed the efficient recyclability of **TAC3**, retaining high performance across six successive adsorption-desorption cycles. In aqueous media, the copolymers also showed promising iodine adsorption, with capacities reaching 5.95 g g^{-1} in I_2 solutions and 5.34 g g^{-1} in I_3^- (KI/I_2) solutions. These conjugated copolymers offer multiple benefits, including ease of synthesis, outstanding chemical and thermal stability, and substantial potential for environmental remediation, as evidenced by their high iodine adsorption capacities.

Data availability

On behalf of my co-authors, I hereby attest that the datasets generated and analyzed during the current study are available from the corresponding author upon request.

Conflicts of interest

There are no conflicts to declare.

Acknowledgements

The project was partially supported by the Kuwait Foundation for the Advancement of Sciences (KFAS) under project code PN18-14SC-03.

References

- 1 N. N. Ponomarev-Stepnoi, V. V. Kuznetsov, A. Y. Gagarinskii, E. J. Moniz, R. Gottemoeller and D. Poneman, The Future of Nuclear Power: Energy, Ecology, and Safety, *At. Energy*, 2002, **93**(5), 855–865, DOI: [10.1023/A:1022400419098](https://doi.org/10.1023/A:1022400419098).
- 2 U. Davies, T. Kunchev, P. Cosgrove, N. Read, M. Kowalski and E. Shwageraus, Nuclear energy: Between global electricity demand, worldwide decarbonisation imperativeness, and planetary environmental implications, *J. Environ. Manage.*, 2019, **249**, 109208, DOI: [10.1016/j.jenvman.2019.06.109](https://doi.org/10.1016/j.jenvman.2019.06.109).
- 3 A. Saiz-Lopez, J. M. C. Plane, A. R. Baker, L. J. Carpenter, R. von Glasow, J. C. Gómez Martín, G. McFiggans and R. W. Saunders, Atmospheric Chemistry of Iodine, *Chem. Rev.*, 2012, **112**(3), 1773–1804, DOI: [10.1021/cr200029u](https://doi.org/10.1021/cr200029u).
- 4 F. C. Küpper, M. C. Feiters, B. Olofsson, T. Kaiho, S. Yanagida, M. B. Zimmermann, L. J. Carpenter, G. W. Luther III, Z. Lu and M. Jonsson, *et al.*, Commemorating Two Centuries of Iodine Research: An Interdisciplinary Overview of Current Research, *Angew. Chem., Int. Ed.*, 2011, **50**(49), 11598–11620, DOI: [10.1002/anie.201100028](https://doi.org/10.1002/anie.201100028).
- 5 L. Thurakkal, S. R. Cheekatla and M. Porel, Superfast Capture of Iodine from Air, Water, and Organic Solvent by Potential Dithiocarbamate-Based Organic Polymer, *Int. J. Mol. Sci.*, 2023, **24**(2), 1466, DOI: [10.3390/ijms24021466](https://doi.org/10.3390/ijms24021466).
- 6 M. Little, G. Kendall, A. Bouville and S. Simon, Measurement of Fukushima-related radioactive contamination in aquatic species, *Proc. Natl. Acad. Sci. U. S. A.*, 2016, **113**, 3720–3721, DOI: [10.1073/pnas.1602648113](https://doi.org/10.1073/pnas.1602648113).
- 7 J. Zhou, T. Lan, T. Li, Q. Chen, P. Bai, F. Liu, Z. Yuan, W. Zheng, X. Luo and W. Yan, *et al.*, Highly efficient capture of iodine in spent fuel reprocessing off-gas by novelly porous copper-doped silica zeolites, *Sep. Purif. Technol.*, 2022, **290**, 120895, DOI: [10.1016/j.seppur.2022.120895](https://doi.org/10.1016/j.seppur.2022.120895).
- 8 H. Xiao, H. Zhou, S. Feng, D. B. Gore, Z. Zhong and W. Xing, In situ growth of two-dimensional ZIF-L nanoflakes on ceramic membrane for efficient removal of iodine, *J. Membr. Sci.*, 2021, **619**, 118782, DOI: [10.1016/j.memsci.2020.118782](https://doi.org/10.1016/j.memsci.2020.118782).
- 9 R. Gao, Y. Lu, S. Xiao and J. Li, Facile Fabrication of Nanofibrillated Chitin/Ag₂O Heterostructured Aerogels with High Iodine Capture Efficiency, *Sci. Rep.*, 2017, **7**(1), 4303, DOI: [10.1038/s41598-017-04436-8](https://doi.org/10.1038/s41598-017-04436-8).
- 10 A. P. Katsoulidis, J. He and M. G. Kanatzidis, Functional Monolithic Polymeric Organic Framework Aerogel as Reducing and Hosting Media for Ag nanoparticles and Application in Capturing of Iodine Vapors, *Chem. Mater.*, 2012, **24**(10), 1937–1943, DOI: [10.1021/cm300696g](https://doi.org/10.1021/cm300696g).
- 11 X. Zhang, J. Maddock, T. M. Nenoff, M. A. Denecke, S. Yang and M. Schröder, Adsorption of iodine in metal-organic framework materials, *Chem. Soc. Rev.*, 2022, **51**(8), 3243–3262, DOI: [10.1039/D0CS01192D](https://doi.org/10.1039/D0CS01192D).
- 12 D. F. Sava, M. A. Rodriguez, K. W. Chapman, P. J. Chupas, J. A. Greathouse, P. S. Crozier and T. M. Nenoff, Capture of volatile iodine, a gaseous fission product, by zeolitic imidazolate framework-8, *J. Am. Chem. Soc.*, 2011, **133**(32), 12398–12401, DOI: [10.1021/ja204757x](https://doi.org/10.1021/ja204757x).
- 13 Z. Yin, Q.-X. Wang and M.-H. Zeng, Iodine Release and Recovery, Influence of Polyiodide Anions on Electrical Conductivity and Nonlinear Optical Activity in an Interdigitated and Interpenetrated Bipillared-Bilayer Metal-Organic Framework, *J. Am. Chem. Soc.*, 2012, **134**(10), 4857–4863, DOI: [10.1021/ja211381e](https://doi.org/10.1021/ja211381e).
- 14 P. Wang, Q. Xu, Z. Li, W. Jiang, Q. Jiang and D. Jiang, Exceptional Iodine Capture in 2D Covalent Organic Frameworks, *Adv. Mater.*, 2018, **30**(29), 1801991, DOI: [10.1002/adma.201801991](https://doi.org/10.1002/adma.201801991).
- 15 S. Huang, J. Y. Choi, Q. Xu, Y. Jin, J. Park and W. Zhang, Carbazolylene-Ethyneylene Macrocycle based Conductive Covalent Organic Frameworks, *Angew. Chem., Int. Ed.*, 2023, **62**(22), e202303538, DOI: [10.1002/anie.202303538](https://doi.org/10.1002/anie.202303538).
- 16 J. Zhou, S. Hao, L. Gao and Y. Zhang, Study on Adsorption Performance of Coal Based Activated Carbon to Radioactive Iodine and Stable Iodine, *Ann. Nucl. Energy*, 2014, **72**, 237–241, DOI: [10.1016/j.anucene.2014.05.028](https://doi.org/10.1016/j.anucene.2014.05.028).
- 17 K. Su, W. Wang, B. Li and D. Yuan, Azo-Bridged Calix[4]-resorcinarene-Based Porous Organic Frameworks with



Highly Efficient Enrichment of Volatile Iodine, *ACS Sustainable Chem. Eng.*, 2018, **6**(12), 17402–17409, DOI: [10.1021/acssuschemeng.8b05203](https://doi.org/10.1021/acssuschemeng.8b05203).

18 J. F. Kurisingal, H. Yun and C. S. Hong, Porous Organic Materials for Iodine Adsorption, *J. Hazard. Mater.*, 2023, **458**, 131835, DOI: [10.1016/j.jhazmat.2023.131835](https://doi.org/10.1016/j.jhazmat.2023.131835).

19 K. Jie, Y. Zhou, E. Li, Z. Li, R. Zhao and F. Huang, Reversible Iodine Capture by Nonporous Pillar[6]arene Crystals, *J. Am. Chem. Soc.*, 2017, **139**(43), 15320–15323, DOI: [10.1021/jacs.7b09850](https://doi.org/10.1021/jacs.7b09850).

20 D. Luo, Y. He, J. Tian, J. L. Sessler and X. Chi, Reversible Iodine Capture by Nonporous Adaptive Crystals of a Bipyridine Cage, *J. Am. Chem. Soc.*, 2022, **144**(1), 113–117, DOI: [10.1021/jacs.1c11731](https://doi.org/10.1021/jacs.1c11731).

21 S. Xiong, X. Tang, C. Pan, L. Li, J. Tang and G. Yu, Carbazole-Bearing Porous Organic Polymers with a Mulberry-Like Morphology for Efficient Iodine Capture, *ACS Appl. Mater. Interfaces*, 2019, **11**(30), 27335–27342, DOI: [10.1021/acsmami.9b07679](https://doi.org/10.1021/acsmami.9b07679).

22 X. Pan, C. Ding, Z. Zhang, H. Ke and G. Cheng, Functional Porous Organic Polymer with High S and N for Reversible Iodine Capture, *Microporous Mesoporous Mater.*, 2020, **300**, 110161, DOI: [10.1016/j.micromeso.2020.110161](https://doi.org/10.1016/j.micromeso.2020.110161).

23 Y. Wu, Y. Guo, R. Su, X. Ma, Q. Wu, Z. Zeng, L. Li, X. Yao and S. Wang, Hierarchical Porous Carbon with an Ultrahigh Surface Area for High-efficient Iodine Capture: Insights into adsorption mechanisms through experiments, simulations and modeling, *Sep. Purif. Technol.*, 2022, **303**, 122237, DOI: [10.1016/j.seppur.2022.122237](https://doi.org/10.1016/j.seppur.2022.122237).

24 S. Pourebrahimi, M. Pirooz, A. De Visscher and G. H. Peslherbe, Highly Efficient and Reversible Iodine Capture Utilizing Amorphous Conjugated Covalent Triazine-based Porous Polymers: Experimental and computational studies, *J. Environ. Chem. Eng.*, 2022, **10**(3), 107805, DOI: [10.1016/j.jece.2022.107805](https://doi.org/10.1016/j.jece.2022.107805).

25 L. Zhang, Y.-T. Luo, J.-Q. Fan, S.-J. Xiao, Q.-Q. Zheng, X.-L. Liu, Q.-G. Tan, C. Sun, Q. Shi and R.-P. Liang, *et al.*, Efficient Capture of Iodine in Steam and Water Media by Hydrogen Bond-driven Charge Transfer Complexes, *J. Hazard. Mater.*, 2024, **465**, 133488, DOI: [10.1016/j.jhazmat.2024.133488](https://doi.org/10.1016/j.jhazmat.2024.133488).

26 J. Huve, A. Ryzhikov, H. Nouali, V. Lalia, G. Augé and T. J. Daou, Porous Sorbents for the Capture of Radioactive Iodine Compounds: a review, *RSC Adv.*, 2018, **8**(51), 29248–29273, DOI: [10.1039/C8RA04775H](https://doi.org/10.1039/C8RA04775H).

27 T. J. Robshaw, J. Turner, S. Kearney, B. Walkley, C. A. Sharrad and M. D. Ogden, Capture of Aqueous Radio-iodine Species by Metallated Adsorbents from Waste-streams of the Nuclear Power Industry: a review, *SN Appl. Sci.*, 2021, **3**(11), 843, DOI: [10.1007/s42452-021-04818-8](https://doi.org/10.1007/s42452-021-04818-8).

28 Y.-N. Yu, Z. Yin, L.-H. Cao and Y.-M. Ma, Organic Porous Solid as Promising Iodine Capture Materials, *J. Inclusion Phenom. Macrocyclic Chem.*, 2022, **102**, 1–33, DOI: [10.1007/s10847-022-01128-3](https://doi.org/10.1007/s10847-022-01128-3).

29 X. Li, Z. Jia, J. Zhang, Y. Zou, B. Jiang, Y. Zhang, K. Shu, N. Liu, Y. Li and L. Ma, Moderate and Universal Synthesis of Undoped Covalent Organic Framework Aerogels for Enhanced Iodine Uptake, *Chem. Mater.*, 2022, **34**(24), 11062–11071, DOI: [10.1021/acs.chemmater.2c03117](https://doi.org/10.1021/acs.chemmater.2c03117).

30 X. Yang, C. Li, M. Giorgi, D. Siri, X. Bugaut, B. Chatelet, D. Gigmes, M. Yemloul, V. Hornebecq and A. Kermagoret, *et al.*, Energy-Efficient Iodine Uptake by a Molecular Host Guest Crystal, *Angew. Chem., Int. Ed.*, 2022, **61**(49), e202214039, DOI: [10.1002/anie.202214039](https://doi.org/10.1002/anie.202214039).

31 W. Zhou, A. Li, M. Zhou, Y. Xu, Y. Zhang and Q. He, Nonporous Amorphous Superadsorbents for Highly Effective and Selective Adsorption of Iodine in Water, *Nat. Commun.*, 2023, **14**(1), 5388, DOI: [10.1038/s41467-023-41056-5](https://doi.org/10.1038/s41467-023-41056-5).

32 Y. Lin, X. Jiang, S. T. Kim, S. B. Alahakoon, X. Hou, Z. Zhang, C. M. Thompson, R. A. Smaldone and C. Ke, An Elastic Hydrogen-Bonded Cross-Linked Organic Framework for Effective Iodine Capture in Water, *J. Am. Chem. Soc.*, 2017, **139**(21), 7172–7175, DOI: [10.1021/jacs.7b03204](https://doi.org/10.1021/jacs.7b03204).

33 A. Gogia, P. Das and S. Mandal, Tunable Strategies Involving Flexibility and Angularity of Dual Linkers for a 3D Metal-Organic Framework Capable of Multimedia Iodine Capture, *ACS Appl. Mater. Interfaces*, 2020, **12**(41), 46107–46118, DOI: [10.1021/acsmami.0c13094](https://doi.org/10.1021/acsmami.0c13094).

34 A. Sen, S. Sharma, S. Dutta, M. M. Shirolkar, G. K. Dam, S. Let and S. K. Ghosh, Functionalized Ionic Porous Organic Polymers Exhibiting High Iodine Uptake from Both the Vapor and Aqueous Medium, *ACS Appl. Mater. Interfaces*, 2021, **13**(29), 34188–34196, DOI: [10.1021/acsmami.1c07178](https://doi.org/10.1021/acsmami.1c07178).

35 D. An, L. Li, Z. Zhang, A. M. Asiri, K. A. Alamry and X. Zhang, Amino-bridged Covalent Organic Polycalix[4]arenes for Ultra Efficient Adsorption of Iodine in Water, *Mater. Chem. Phys.*, 2020, **239**, 122328, DOI: [10.1016/j.matchemphys.2019.122328](https://doi.org/10.1016/j.matchemphys.2019.122328).

36 Z. Chen, K. B. Idrees, S. Shetty, H. Xie, M. C. Wasson, W. Gong, X. Zhang, B. Alameddine and O. K. Farha, Regulation of Catenation in Metal-Organic Frameworks with Tunable Clathrochelate-Based Building Blocks, *Cryst. Growth Des.*, 2021, **21**(12), 6665–6670, DOI: [10.1021/acs.cgd.1c01151](https://doi.org/10.1021/acs.cgd.1c01151).

37 B. Alameddine, S. Shetty, R. S. Anju, F. Al-Sagheer and S. Al-Mousawi, Highly Soluble Metal-organic Polymers Based on Iron(II) clathrochelates and their Gelation Induced by Sono-citation, *Eur. Polym. J.*, 2017, **95**, 566–574, DOI: [10.1016/j.eurpolymj.2017.08.049](https://doi.org/10.1016/j.eurpolymj.2017.08.049).

38 S. Shetty, N. Baig, S. Al-Mousawi, F. Al-Sagheer and B. Alameddine, Synthesis of Secondary Arylamine Copolymers with Iron(II) Clathrochelate Units and their Functionalization into Tertiary Polyarylamines via Buchwald–Hartwig Cross-coupling reaction, *Polymer*, 2019, **178**, 121606, DOI: [10.1016/j.polymer.2019.121606](https://doi.org/10.1016/j.polymer.2019.121606).

39 S. M. Jansze and K. Severin, Clathrochelate Metalloligands in Supramolecular Chemistry and Materials Science, *Acc. Chem. Res.*, 2018, **51**(9), 2139–2147, DOI: [10.1021/acs.accounts.8b00306](https://doi.org/10.1021/acs.accounts.8b00306).

40 O. A. Varzatskii, I. N. Denisenko, S. V. Volkov, A. V. Dolganov, A. V. Vologzhanina, Y. N. Bubnov and Y. Z. Voloshin, First Example of Perfluoroalkylation of a Quasi-aromatic Encapsulating ligand: 2,5-Dithiahexane-assisted Reaction of the Iron(II) diiodoclathrochelate with Trifluoromethylcopper(I), *Inorg. Chem. Commun.*, 2013, **33**, 147–150, DOI: [10.1016/j.inoche.2013.04.024](https://doi.org/10.1016/j.inoche.2013.04.024).



41 B. Alameddine, S. Shetty, N. Baig, S. Al-Mousawi and F. Al-Sagheer, Synthesis and Characterization of Metalorganic Polymers of Intrinsic Microporosity Based on Iron(II) Clathrochelate, *Polymer*, 2017, **122**, 200–207, DOI: [10.1016/j.polymer.2017.06.048](https://doi.org/10.1016/j.polymer.2017.06.048).

42 S. Shetty, K. B. Idrees, H. Xie, B. Alameddine and O. K. Farha, Synthesis of Zirconium-based Metal-organic Frameworks with Iron(II) Clathrochelate Ligands, *CrystEngComm*, 2023, **25**(10), 1550–1555, DOI: [10.1039/D2CE01686A](https://doi.org/10.1039/D2CE01686A).

43 S. Shetty, N. Baig, A. Hassan, S. Al-Mousawi, N. Das and B. Alameddine, Fluorinated Iron(II) Clathrochelate Units in Metalorganic Based Copolymers: Improved Porosity, Iodine Uptake, and Dye Adsorption Properties, *RSC Adv.*, 2021, **11**(25), 14986–14995, DOI: [10.1039/D1RA02357H](https://doi.org/10.1039/D1RA02357H).

44 S. Shetty, N. Baig, S. Al-Mousawi and B. Alameddine, Removal of Anionic and Cationic Dyes Using Porous Copolymer Networks Made from a Sonogashira Cross-coupling Reaction of Diethynyl Iron(II) clathrochelate with Various Arylamines, *J. Appl. Polym. Sci.*, 2022, **139**(43), e52966, DOI: [10.1002/app.52966](https://doi.org/10.1002/app.52966).

45 W. Gong, Y. Xie, T. D. Pham, S. Shetty, F. A. Son, K. B. Idrees, Z. Chen, H. Xie, Y. Liu and R. Q. Snurr, *et al.*, Creating Optimal Pockets in a Clathrochelate-Based Metal-Organic Framework for Gas Adsorption and Separation: Experimental and Computational Studies, *J. Am. Chem. Soc.*, 2022, **144**(8), 3737–3745, DOI: [10.1021/jacs.2c00011](https://doi.org/10.1021/jacs.2c00011).

46 N. Baig, S. Shetty, R. Bargakshatriya, S. K. Pramanik and B. Alameddine, Efficient Removal of Carcinogenic Azo Dyes from Water Using Iron(II) Clathrochelate Derived Metalorganic Copolymers Made from a Copper-Catalyzed [4+2] Cyclobenzannulation Reaction, *Polymers*, 2023, **15**(13), 2948, DOI: [10.3390/polym15132948](https://doi.org/10.3390/polym15132948).

47 S. Shetty, N. Baig, M. Bechelany and B. Alameddine, Construction of Polyimide Structures Containing Iron(II) Clathrochelate Intercalators: Promising Materials for CO₂ Gas Uptake and Salient Adsorbents of Iodine from Gaseous and Liquid Phases, *J. Mater. Chem. A*, 2024, **12**(23), 14059–14071, DOI: [10.1039/D4TA02194K](https://doi.org/10.1039/D4TA02194K).

48 C. Zhao, L. Ge, M. Zuo, L. Mai, S. Chen, X. Li, Q. Li, Y. Wang and C. Xu, Study on the mechanical strength and iodine adsorption behavior of coal-based activated carbon based on orthogonal experiments, *Energy*, 2023, **282**, 128450, DOI: [10.1016/j.energy.2023.128450](https://doi.org/10.1016/j.energy.2023.128450).

49 J. Cheng, B. Gao, H. Tang, Z. Sun, L. Xu, L. Wang and D. Cao, Hexnut[12]arene and its derivatives: Synthesis, host-guest properties, and application as nonporous adaptive crystals, *Sci. China:Chem.*, 2022, **65**(3), 539–545, DOI: [10.1007/s11426-021-1186-2](https://doi.org/10.1007/s11426-021-1186-2).

50 A. Mohan, M. Al-Sayah, A. Ahmed and O. El-Kadri, Triazine-based porous organic polymers for reversible capture of iodine and utilization in antibacterial application, *Sci. Rep.*, 2022, **12**, 2638, DOI: [10.1038/s41598-022-06671-0](https://doi.org/10.1038/s41598-022-06671-0).

51 Y. Matsumoto and K. Honma, NH stretching vibrations of pyrrole clusters studied by infrared cavity ringdown spectroscopy, *J. Chem. Phys.*, 2007, **127**, 184310, DOI: [10.1063/1.2790894](https://doi.org/10.1063/1.2790894).

52 S. Shetty, N. Baig, D. Sengupta, O. K. Farha and B. Alameddine, Tröger's Base-Enriched Conjugated Cyclopentannulated Copolymers: Prominent Adsorbents of CO₂, H₂, and Iodine, *ACS Appl. Mater. Interfaces*, 2024, **16**(6), 8130–8139, DOI: [10.1021/acsami.3c18055](https://doi.org/10.1021/acsami.3c18055).

53 M. Tommasini, A. Lucotti, M. Alfè, A. Ciajolo and G. Zerbi, Fingerprints of polycyclic aromatic hydrocarbons (PAHs) in infrared absorption spectroscopy, *Spectrochim. Acta, Part A*, 2016, **152**, 134–148, DOI: [10.1016/j.saa.2015.07.070](https://doi.org/10.1016/j.saa.2015.07.070).

54 M. Slaný, L. Jankovič and J. Madejová, Near-IR study of the impact of alkyl-ammonium and -phosphonium cations on the hydration of montmorillonite, *J. Mol. Struct.*, 2022, **1256**, 132568, DOI: [10.1016/j.molstruc.2022.132568](https://doi.org/10.1016/j.molstruc.2022.132568).

55 L. Rintoul, A. S. Micallef and S. E. Bottle, The vibrational group frequency of the N–O stretching band of nitroxide stable free radicals, *Spectrochim. Acta, Part A*, 2008, **70**(4), 713–717, DOI: [10.1016/j.saa.2007.08.017](https://doi.org/10.1016/j.saa.2007.08.017).

56 N. Baig, S. Shetty, S. S. Habib, A. A. Husain, S. Al-Mousawi and B. Alameddine, Synthesis of Iron(II) Clathrochelate-Based Poly(vinylene sulfide) with Tetraphenylbenzene Bridging Units and Their Selective Oxidation into Their Corresponding Poly(vinylene sulfone) Copolymers: Promising Materials for Iodine Capture, *Polymers*, 2022, **14**(18), 3727, DOI: [10.3390/polym14183727](https://doi.org/10.3390/polym14183727).

57 O. Yildirim, A. Tsaturyan, A. Damin, S. Nejrotti, V. Crocellà, A. Gallo, M. R. Chierotti, M. Bonomo and C. Barolo, Quinoid-Thiophene-Based Covalent Organic Polymers for High Iodine Uptake: When Rational Chemical Design Counterbalances the Low Surface Area and Pore Volume, *ACS Appl. Mater. Interfaces*, 2023, **15**(12), 15819–15831, DOI: [10.1021/acsami.2c20853](https://doi.org/10.1021/acsami.2c20853).

58 S. S. AlNeyadi, M. T. Alhassani, A. S. Aleissae, Sultan J., A. H. Khalaf, A. A. Alteneij and Y. Y. Alyaarbi, Synthesizing covalent organic frameworks for unprecedented iodine capture performance, *Heliyon*, 2024, **10**(4), e25921, DOI: [10.1016/j.heliyon.2024.e25921](https://doi.org/10.1016/j.heliyon.2024.e25921).

59 Y. Xie, T. Pan, Q. Lei, C. Chen, X. Dong, Y. Youyou, J. Shen, Y. Cai, C. Zhou and I. Pinnau, *et al.*, Ionic Functionalization of Multivariate Covalent Organic Frameworks to Achieve Exceptionally High Iodine Capture Capacity, *Angew. Chem.*, 2021, **133**(41), 22606–22614, DOI: [10.1002/ange.202108522](https://doi.org/10.1002/ange.202108522).

60 J. Wang, T. Wu, X. Wang, J. Chen, M. Fan, Z. Shi, J. Liu, L. Xu and Y. Zang, Construction of hydroxyl-functionalized hyper-crosslinked networks from polyimide for highly efficient iodine adsorption, *iScience*, 2024, **27**(2), 108993, DOI: [10.1016/j.isci.2024.108993](https://doi.org/10.1016/j.isci.2024.108993).

61 C. Li, Q. Yan, H. Xu, S. Luo, H. Hu, S. Wang, X. Su, S. Xiao and Y. Gao, Highly Efficient Capture of Volatile Iodine by Conjugated Microporous Polymers Constructed Using Planar 3- and 4-Connected Organic Monomers, *Molecules*, 2024, **29**(10), 2242, DOI: [10.3390/molecules29102242](https://doi.org/10.3390/molecules29102242).

62 F. Begar, M. Erdogan, Y. Gecalp, U. C. Canakci and O. Buyukcevikir, Synthesis of Triazole-Linked Porous Cage Polymers: Modulating Cage Size for Tailored Iodine Adsorption, *ACS Appl. Polym. Mater.*, 2024, **6**(9), 5358–5365, DOI: [10.1021/acsapm.4c00560](https://doi.org/10.1021/acsapm.4c00560).



63 S. Luo, Q. Yan, S. Wang, H. Hu, S. Xiao, X. Su, H. Xu and Y. Gao, Conjugated Microporous Polymers Based on Octet and Tetratopic Linkers for Efficient Iodine Capture, *ACS Appl. Mater. Interfaces*, 2023, **15**(39), 46408–46416, DOI: [10.1021/acsami.3c10786](https://doi.org/10.1021/acsami.3c10786).

64 C.-H. Zhang, B.-X. Zhou, X. Lin, J.-X. Wu, L.-H. Wu, S. Cai, J. Fan, W.-G. Zhang, Y. Yan and S.-R. Zheng, High-Capacity Iodine Adsorption and Nonporous to Porous Structural Transformation in an Originally Nonporous Coordination Polymer, *Inorg. Chem. Front.*, 2024, **11**(3), 769–778, DOI: [10.1039/D3QI01881D](https://doi.org/10.1039/D3QI01881D).

65 H. Zhu, Y. Qin, Y. Guo, Z. Shen, M. Imran, M. Asim Mushtaq, Z. Zhang, C. Ni, Y. Chen and Y. Ding, *et al.*, Covalent organic polymers for efficient removal of iodine from gas- and liquid-phase environments, *Chem. Eng. J.*, 2024, **484**, 149739, DOI: [10.1016/j.cej.2024.149739](https://doi.org/10.1016/j.cej.2024.149739).

66 B. Liu, C. Mao, Z. Zhou, Q. Wang, X. Zhou, Z. Liao, R. Deng, D. Liu, J. Beiyuan and D. Lv, *et al.*, Two Facile Aniline-Based Hypercrosslinked Polymer Adsorbents for Highly Efficient Iodine Capture and Removal, *Int. J. Mol. Sci.*, 2023, **24**(1), 370, DOI: [10.3390/ijms24010370](https://doi.org/10.3390/ijms24010370).

67 Y. H. Abdelmoaty, T. D. Tessema, F. A. Choudhury, O. M. El-Kadri and H. M. El-Kaderi, Nitrogen-Rich Porous Polymers for Carbon Dioxide and Iodine Sequestration for Environmental Remediation, *ACS Appl. Mater. Interfaces*, 2018, **10**(18), 16049–16058, DOI: [10.1021/acsami.8b03772](https://doi.org/10.1021/acsami.8b03772).

68 N. Arora, T. Debnath, M. C. Senarathna, R. M. Johnson, I. G. Roske, G. A. Cisneros and R. A. Smaldone, Rapid, high-capacity adsorption of iodine from aqueous environments with amide functionalized covalent organic frameworks, *Chem. Sci.*, 2024, **15**(10), 3571–3577, DOI: [10.1039/D3SC06004G](https://doi.org/10.1039/D3SC06004G).

69 A. Mohan, M. H. Al-Sayah, A. Ahmed and O. M. El-Kadri, Triazine-based porous organic polymers for reversible capture of iodine and utilization in antibacterial application, *Sci. Rep.*, 2022, **12**(1), 2638, DOI: [10.1038/s41598-022-06671-0](https://doi.org/10.1038/s41598-022-06671-0).

70 Z. Yan, Y. Yuan, Y. Tian, D. Zhang and G. Zhu, Highly Efficient Enrichment of Volatile Iodine by Charged Porous Aromatic Frameworks with Three Sorption Sites, *Angew. Chem., Int. Ed.*, 2015, **54**(43), 12733–12737, DOI: [10.1002/anie.201503362](https://doi.org/10.1002/anie.201503362).

71 M. Ansari, A. Alam, R. Bera, A. Hassan, S. Goswami and N. Das, Synthesis, characterization and adsorption studies of a novel triptycene based hydroxyl azo- nanoporous polymer for environmental remediation, *J. Environ. Chem. Eng.*, 2020, **8**(2), 103558, DOI: [10.1016/j.jece.2019.103558](https://doi.org/10.1016/j.jece.2019.103558).

72 B. Liu, C. Mao, Z. Zhou, Q. Wang, X. Zhou, Z. Liao, R. Deng, D. Liu, J. Beiyuan and D. Lv, *et al.*, Two Facile Aniline-Based Hypercrosslinked Polymer Adsorbents for Highly Efficient Iodine Capture and Removal, *Int. J. Mol. Sci.*, 2022, **24**(1), 370, DOI: [10.3390/ijms24010370](https://doi.org/10.3390/ijms24010370).

73 T. Geng, M. Liu, C. Zhang, C. Hu and H. Xu, Synthesis of secondary amine-based fluorescent porous organic polymers *via* Friedel–Crafts polymerization reaction for adsorbing and fluorescent sensing iodine, *J. Appl. Polym. Sci.*, 2020, **137**(41), 49255, DOI: [10.1002/app.49255](https://doi.org/10.1002/app.49255).

74 S. Pourebrahimi and M. Pirooz, Functionalized covalent triazine frameworks as promising platforms for environmental remediation: A review, *Cleaner Chem. Eng.*, 2022, **2**, 100012, DOI: [10.1016/j.ccle.2022.100012](https://doi.org/10.1016/j.ccle.2022.100012).

75 C. Feng, G. Xu, W. Xie, S. Zhang, C. Yao and Y. Xu, Polytriazine porous networks for effective iodine capture, *Polym. Chem.*, 2020, **11**(16), 2786–2790, DOI: [10.1039/C9PY01948K](https://doi.org/10.1039/C9PY01948K).

76 H. Zuo, W. Lyu, W. Zhang, Y. Li and Y. Liao, High-Yield Synthesis of Pyridyl Conjugated Microporous Polymer Networks with Large Surface Areas: From Molecular Iodine Capture to Metal-Free Heterogeneous Catalysis, *Macromol. Rapid Commun.*, 2020, **41**(22), 2000489, DOI: [10.1002/marc.202000489](https://doi.org/10.1002/marc.202000489).

77 A. Hassan, A. Alam, S. Chandra, O. Prince and N. Das, Triptycene-based and imine linked porous uniform microspheres for efficient and reversible scavenging of iodine from various media: a systematic study, *Environ. Sci.:Adv.*, 2022, **1**(3), 320–330, DOI: [10.1039/D2VA00024E](https://doi.org/10.1039/D2VA00024E).

78 T. Wang, M. Jiang, X. Yu, N. Niu and L. Chen, Application of lignin adsorbent in wastewater Treatment: A review, *Sep. Purif. Technol.*, 2022, **302**, 122116, DOI: [10.1016/j.seppur.2022.122116](https://doi.org/10.1016/j.seppur.2022.122116).

79 Z.-b Liu, J. Tian, W. Zang, W.-Y. Zhou, F. Song, C.-P. Zhang, J.-Y. Zheng and H. Xu, Flexible alteration of optical nonlinearities of iodine charge-transfer complexes in solutions, *Opt. Lett.*, 2004, **29**, 1099–1101, DOI: [10.1364/OL.29.001099](https://doi.org/10.1364/OL.29.001099).

80 Y. Ji, J. Huang, C. Liu, C. Ni, H. Yan, Y. David and Y. Qin, Introgression of Lone Electron Pairs into π -Conjugated Structures Resulting in Giant Electron-Rich Clusters with High Trapping Capacity for Iodine Molecules, *ACS Appl. Polym. Mater.*, 2024, **6**(13), 7478–7487, DOI: [10.1021/acsapm.4c00816](https://doi.org/10.1021/acsapm.4c00816).

81 H. Fu, Y. Tang, Q. Yuan, J. Chang, F. Liao, J. Zhang, H. Gao, Y. Yang and Y. Liao, Understanding iodine adsorption sites on monolithic N/O co-doped carbon fibers with scaffolding structure, *Fuel*, 2024, **371**, 132035, DOI: [10.1016/j.fuel.2024.132035](https://doi.org/10.1016/j.fuel.2024.132035).

82 S. Bera, K. Garg and S. K. Samanta, Amide-Linked *cis,cis*-1,3,5-Cyclohexanetricarbonyl-Based Porous Organic Polymers for the Uptake of Iodine in Solution and Vapor Phase, *ACS Appl. Nano Mater.*, 2024, **7**(2), 1797–1803, DOI: [10.1021/acsannm.3c04973](https://doi.org/10.1021/acsannm.3c04973).

83 L.-L. Li, M. Huang, T. Chen, X.-F. Xu, Z. Zhuo, W. Wang and Y.-G. Huang, A Porous π -Stacked Self-Assembly of Cup-Shaped Palladium Complex for Iodine Capture, *Molecules*, 2023, **28**(7), 2881, DOI: [10.3390/molecules28072881](https://doi.org/10.3390/molecules28072881).

84 F. Khosravi Esmaeilikhani, M. Dinari and N. Mokhtari, Nitrogen-rich porous organic polymer as a promising adsorbent for iodine capture from organic solvents, *New J. Chem.*, 2024, **48**(5), 1943–1951, DOI: [10.1039/D3NJ04674E](https://doi.org/10.1039/D3NJ04674E).

85 Q. Tao, X. Zhang, L. Jing, L. Sun and P. Dang, Construction of Ketoenamine-Based Covalent Organic Frameworks with Electron-Rich Sites for Efficient and Rapid Removal of Iodine from Solution, *Molecules*, 2023, **28**(24), 8151, DOI: [10.3390/molecules28248151](https://doi.org/10.3390/molecules28248151).

86 L. Xie, Z. Zheng, Q. Lin, H. Zhou, X. Ji, J. L. Sessler and H. Wang, Calix[4]pyrrole-based Crosslinked Polymer Networks for Highly Effective Iodine Adsorption from Water, *Angew. Chem., Int. Ed.*, 2022, **61**(1), e202113724, DOI: [10.1002/anie.202113724](https://doi.org/10.1002/anie.202113724).



87 E. Yazdankish, M. Foroughi and M. H. A. Azqhandi, Capture of I₁₃₁ from medical-based wastewater using the highly effective and recyclable adsorbent of g-C₃N₄ assembled with Mg-Co-Al-layered double hydroxide, *J. Hazard. Mater.*, 2020, **389**, 122151, DOI: [10.1016/j.jhazmat.2020.122151](https://doi.org/10.1016/j.jhazmat.2020.122151).

88 Y. Yin, Y. Yang, G. Liu, H. Chen, D. Gong, Y. Ying, J. Fan, S. Liu, Z. Li and C. Wang, *et al.*, Ultrafast solid-phase synthesis of 2D pyrene-alkadiyne frameworks towards efficient capture of radioactive iodine, *Chem. Eng. J.*, 2022, **441**, 135996, DOI: [10.1016/j.cej.2022.135996](https://doi.org/10.1016/j.cej.2022.135996).

89 M. Avais and S. Chattopadhyay, Porous polyaminoamides *via* an exotemplate synthesis approach for ultrahigh multimedia iodine adsorption, *J. Mater. Chem. A*, 2022, **10**(37), 20090–20100, DOI: [10.1039/D2TA02708A](https://doi.org/10.1039/D2TA02708A).

90 C. X. Yu, X. J. Li, J. S. Zong, D. J. You, A. P. Liang, Y. L. Zhou, X. Q. Li and L. L. Liu, Fabrication of Protonated Two-Dimensional Metal-Organic Framework Nanosheets for Highly Efficient Iodine Capture from Water, *Inorg. Chem.*, 2022, **61**(35), 13883–13892, DOI: [10.1021/acs.inorgchem.2c01886](https://doi.org/10.1021/acs.inorgchem.2c01886).

91 D. Chen, T. Ma, X. Zhao, X. Jing, R. Zhao and G. Zhu, Multi-Functionalization Integration into the Electrospun Nanofibers Exhibiting Effective Iodine Capture from Water, *ACS Appl. Mater. Interfaces*, 2022, **14**(41), 47126–47135, DOI: [10.1021/acsami.2c14724](https://doi.org/10.1021/acsami.2c14724).

92 X.-H. Xu, Y.-X. Li, L. Zhou, N. Liu and Z.-Q. Wu, Precise fabrication of porous polymer frameworks using rigid polyisocyanides as building blocks: from structural regulation to efficient iodine capture, *Chem. Sci.*, 2022, **13**(4), 1111–1118, DOI: [10.1039/D1SC05361B](https://doi.org/10.1039/D1SC05361B).

93 P. Samanta, S. Dutta, S. Let, A. Sen, M. M. Shirolkar and S. K. Ghosh, Hydroxy-Functionalized Hypercrosslinked Polymers (HCPs) as Dual Phase Radioactive Iodine Scavengers: Synergy of Porosity and Functionality, *ChemPlusChem*, 2022, **87**(11), e202200212, DOI: [10.1002/cplu.202200212](https://doi.org/10.1002/cplu.202200212).

94 M. Das, S. Sarkar, Y. Patra, A. Manna, S. Mukherjee and S. Das, Soft Self-Templating Approach-Derived Covalent Triazine Framework with Bimodal Nanoporosity for Efficient Radioactive Iodine Capture for Safe Nuclear Energy, *ACS Appl. Nano Mater.*, 2022, **5**(7), 8783–8793, DOI: [10.1021/acsanm.2c00564](https://doi.org/10.1021/acsanm.2c00564).

